IEEE Access
Multidisciplinary | Rapid Review | Open Access Journal

Received 20 March 2024, accepted 16 April 2024, date of publication 20 May 2024, date of current version 18 June 2024.

Digital Object Identifier 10.1109/ACCESS.2024.3402958

RESEARCH ARTICLE

SER Reduction in NLOS MM Wave Links Using Minimally Equicorrelated MIMO-MRC System

SABYASACHI BHATTACHARYYA AND G. ARUNA
Department of Electronics and Communication Engineering, Indian Institute of Information Technology Guwahati, Guwahati 781015, India
Corresponding author: Sabyasachi Bhattacharyya (sabya005@gmail.com)

ABSTRACT 5G and next-generation physical layer advancements have being made at a breakneck speed. At the heart of it is millimeter wave technology, which uses extremely high frequency transmissions at 28, 38, and 72 GHz. These MM wave channels utilize approximately 20 GHz of spare spectrum to enable faster data rates to a larger number of mobile subscribers. In multiple-input multiple-output (MIMO) systems, transmit beamsteering through directional antenna arrays supported by maximal ratio combining (MRC) receivers is used alongwith MM wave technology to investigate link performance as a function of unfavourable inter-antenna correlations. In this paper, the system is modelled for short-range MM wave communications under separately correlated, non-line-of-sight (NLOS) Rayleigh environments. Here, exact closed form expressions are presented for the symbol error rate (SER) and asymptotic (high signal-to-noise ratio (SNR)) SER of the beamsteered MM wave model. The dependency of SER on transmit-receive correlations is seen in the derivations. The results are analyzed using double-correlated statistics for the maximum eigen value of complex Wishart matrices. Specifically, in the MM wave regime, correlation matrix entries vary with steering/response vectors. This does not hold true in the case of microwave links. It is therefore proposed to effectively adjust these vectors to attain novel minimized equicorrelations at the transmit and receive sides of the MM wave MIMO link. The minimally tuned MIMO-MRC model demonstrates significant average SER and asymptotic (high SNR) SER reductions under both uplink and downlink scenarios with two (02) antennas at the transmitter and receiver, respectively. The proposed model also showcases drastically lower average SER levels compared to those of existing non-equicorrelated systems. Simulation results validate the analytical study.

INDEX TERMS Minimal equicorrelations, millimeter wave, eigen value, MIMO modeling, symbol error rate.

I. INTRODUCTION

Millimeter (MM) wave systems have emerged as an integral part of future-generation wireless communications. The thrust of achieving increased capacity levels with exceedingly low error rates to support cutting-edge multimedia applications can be fulfilled by communicating at MM wave frequencies [1], [2], [3], [4], [5], [6], [7], [8], [9], [10], [11], [12], [13], [14], [15], [16], [17], [18], [19], [20], [21], [22], [23], [24], [25], [26], [27]. Approximately 20 GHz of free spectrum is available in the 28, 38, and 72 GHz bands [2], [7], [28], [29], [30], [31], [32], [33], [34], [35], [36], [37], [38], [39], [40], [41], [42], [43]. This huge operating spectrum could be utilised to serve a higher number of cellular users at enhanced data rates with various data modulation formats. When compared to 4G microwave links, millimetre wave transmissions are expected to produce a hundred-fold increase in capacity measures with significantly lower error levels [5], [38], [44], [45], [46], [47], [48], [49], [50], [51], [52], [53], [54]. Phased array systems also provide increased capacity through enhanced directivity gains. As MM wave links operate at higher GHz frequencies, antenna dimensions will be in millimeters, leading to phased arrays on chip. The SNR at receiver output is a key to error analysis in such MIMO links [9], [55], [56], [57], [58], [59], [60], [61], [62], [63]. Of late, various challenges related to signal processing

The associate editor coordinating the review of this manuscript and approving it for publication was Jiayi Zhang.

for MM wave performance gains have been emphasised [12], [64], [65], [66], [67], [68], [69]. Some related works are discussed below.

Sooyoung et al.'s outdoor inter-cell backhaul and intra-cell mobile access proposal in [1], Janssen's impulse response based system bit error rate (BER) analysis in [2], Rappaport et al.'s experimental analysis on path loss and angle of arrival (AoA) considering beamsteered arrays in [4], Heath et al.'s novel proposal of both 2-D and 3-D channel models for a beamsteered Uniform Linear Array (ULA) with N antennas in [5], Niu et al.'s comparison with microwave transmissions taking into account bottlenecks such as blockage sensitivity, increased losses, directional dependance in [6] and Alkhateeb's multi-resolution, recursive algorithm for optimal beamforming in [7] and [8] are solely dependant on MM wave channel statistics and do not utilize correlation based receiver statistics.

To devise MM wave performance improvement techniques, receiver statistics also play a dominant role, in addition to vital channel statistics [6], [7]. The performance of MIMO systems is hugely degraded by inter-antenna correlations in the MM wave regime [62], [69]. To overcome the same, statistical characterization of MIMO receiver parameters in terms of correlation measures is a must [1].

In this direction, [10] presents generic NLOS MIMO receiver parameters in terms of separate transmit-receive (Kronecker) correlations whereas [11], [12] investigate correlated channel limits besides introducing MIMO equicorrelations for achieving correlation control (and thereby improved channel bounds/receiver performance) in such systems. Of late, marginal correlated LOS Massive MIMO performance improvements have been achieved by Hemadeh et al. under MM wave regime in [62] using the popular Saleh Valenzuela (SV) physical channel model [68] and by Bjornson et al. with sub-6 GHz as well as MM wave carriers in [69].

MM wave propagations are predominantly LOS in nature where it is typical to consider physical models for accurate parameter evaluation [62]. Contrary to this, recent works [60], [61], [63] stress on accurate stochastic correlation modeling for NLOS MM wave performance analysis. Towards this, Ganesan et al.'s learning based obstacle tracking model for Device-to-Device (D2D) communications in [70], Barneto et al.'s regularized least-squares (LS) approach for user location sensing in [71], Karasawa's multistate LOS/NLOS channel model developed using Nakagami-m parameters in [72], Xia et al.'s two-stage generative neural network based model for high resolution channel/receiver parameter estimation in [73], Ju et al.'s 3-D LOS/NLOS channel model built around extensive radio propagation measurements in [74], Zhao et al.'s novel semi-deterministic model based on optimal neural network (ONN) for dynamic channel parameter evaluation in [75] and Lecci et al.'s quasi-deterministic (QD) mathematical framework which generates channel instances precisely matching real 60 GHz measurements in [76] effectively utilize statistical means to study NLOS MM wave receiver performance metrics in terms of spatial correlations.

The research presented in [62], [69], [70], [71], [72], [73], [74], [75], and [76] is however restricted to only analysing MIMO receiver performance in terms of transmitter and receiver correlations. The possibility of tuning MM wave performance by controlling such correlation levels has not been explored which motivated the proposed work. In this direction, the current work reveals that MIMO taps and correlation matrix entries only in the MM wave domain are dependent on steering/response vectors or corresponding departure/arrival angles [5]. This crucial dependency, which does not exist for microwave links, is further utilized in the proposed work by effectively tuning steering angles to achieve novel minimized equicorrelations in MM wave transceivers [10]. Following this, the paper presents a new Minimally Equicorrelated MIMO-MRC model for SER performance improvement under short-range NLOS MM wave channels. Novel closed form expressions are subsequently put forward for the average SER and asymptotic (high SNR) SER of the beamsteered MM wave model. The proposed MIMO-MRC model with minimal equicorrelations showcases significant average SER and asymptotic (high SNR) SER reductions under both uplink and downlink scenarios with two (02) antennas at the transmitter and receiver, respectively. When compared to other non-equicorrelated MM wave models presented in [62], [69], [70], [71], [72], [73], [74], [75], and [76], the proposed system demonstrates much lower average SER levels resulting from equally minimized transmit-receive correlations. The author's key contributions are highlighted as below.

- Previously unexplored dependency of MM wave MIMO taps and correlation matrix entries on tunable steering vectors is presented.
- Novel minimized equicorrelations are achieved in MM wave MIMO-MRC system through effective departure/arrival angle tuning.
- A novel Minimally Equicorrelated MIMO-MRC model with beamsteering for SER performance improvement under short range NLOS MM wave channels is proposed.
- New closed form expressions are put forward for correlated MM wave average SER and asymptotic (high SNR) SER.
- Significant reductions in average SER and asymptotic (high SNR) SER for the minimal equicorrelation model are observed under both uplink and downlink scenarios with similar constraints of maximum two (02) antennas at transmitter and receiver respectively as depicted in [77] and [78].
- The proposed system with minimal transceiver correlation demonstrates drastically lower average SER levels than those of non-equicorrelated MM wave models presented in [62], [69], [70], [71], [72], [73], [74], [75], and [76].

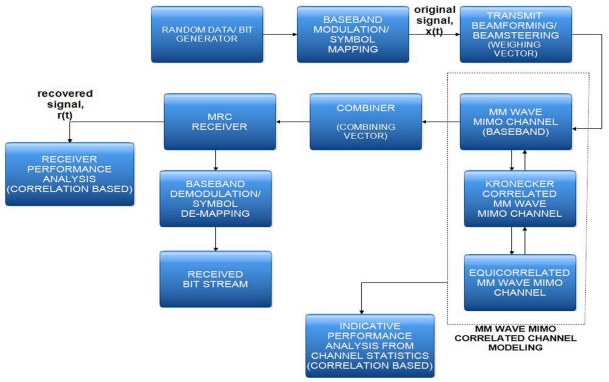

FIGURE 1. Proposed MM Wave System Arrangement.

The remaining portion of this paper is arranged as follows. Section II describes a MM wave MIMO-MRC system for Short range NLOS transmission in terms of the proposed communication model and scenario considerations. Section III discusses Correlated MIMO modeling of MM wave channels. It initially describes chosen MM wave Beamspace MIMO channels followed by stochastic correlation modeling of such links. Section IV illustrates the proposed MM wave MIMO-MRC receiver model for beamsteered short range communications. Section V analyzes the performance of MIMO-MRC under Double Correlated MM wave channels in terms of Average SER and Asymptotic (high SNR) SER. Section VI illustrates the analytical and practical modelling of Minimally Equicorrelated MIMO-MRC links. Section VII presents experimental observations related to performance of the proposed model. Finally, Section VIII summarizes the discussion.

II. SHORT RANGE MIMO-MRC MODEL FOR BEAMSTEERED NLOS MM WAVE COMMUNICATIONS

On the transmit side, beamsteering is incorporated to ensure signal availability for nearby users [5]. Also, MRC-aided detection is utilized at the receiver end [10]. In the MM wave regime, operating wavelengths are quite low and this results in signal transmissions being prominently impacted by inter-antenna correlations modeled here using Kronecker decompositions [9], [10].

A. PROPOSED ARRANGEMENT

The system model is illustrated in Figure 1. We consider a digital information source [27]. The binary bits generated are further subjected to popular modulation methods, namely BPSK, BFSK, 4-PAM, QPSK, etc. [10]. The symbols obtained from baseband modulation are subsequently beamsteered for near-user signal reception [5]. The resultant signal is transmitted through the MM wave baseband MIMO channel [9].

Firstly, Kronecker correlations are incorporated into the MM wave MIMO channel proposed in [5] for analyzing the effect of antenna correlations on receiver performance [11].

TABLE 1. Notations used and their meaning.

S.No.	Notation	Description
1.	$\arcsin(\cdot)$	Inverse sine operation
2.	$[\cdot]^T$	Matrix transpose
3.	$[\cdot]^*$	Element wise matrix conjugate operation
4.	$E[\cdot]$	Expectation operator
5.	$E \bigotimes F$	Kronecker product of matrices E and F
6.	$vect(E)$	Column-wise stacking of E into a single column matrix
7.	$[\cdot]^H$	Matrix Hermitian conjugate
8.	$[\cdot]^{\frac{1}{2}}$	Hermitian matrix square root
9.	$det([\cdot])$	Matrix determinant operation
10.	$[\cdot]^{\frac{H}{2}}$	Composite Matrix Hermitian and Square Root operation
11.	$e^{[\cdot]}$	Exponential function
12.	$[\cdot]^{-1}$	Matrix inversion
13.	$\|J\|^2, \|\|J\|\|^2$	Squared modulus and squared Euclidian norm of vector J
14.	$N_o : \mathcal{CN}_{x,1}(O_{x\times 1}, I_x)$	Complex Normally distributed random variable of size $x \times 1$
15.	$O_{x\times 1}$	All zero vector denoting zero ensemble means
16.	I_x	Diagonal entries of identity matrix showing unity variances
17.	$[F]^\dagger$	Hermitian estimate of matrix F
18.	$cos(\cdot), sin(\cdot)$	Usual cosine and sine operations
19.	$z \sim \mathcal{N}(0, \sigma^2)$	Normally distributed random variable with zero mean and variance σ^2
20.	$g \sim \mathcal{N}_C^n(e, f)$	n-Multivariate, complex, Normally distributed vector with mean vector e and covariance matrix f
21.	$\Delta_k(S)$	k-dimensional Vandermonde determinant of square matrix S
22.	$A^\dagger A$	Wishart matrix for arbitrary matrix A
23.	$\Gamma_n(\cdot)$	Complex Gamma multivariate function
24.	$\wp(\cdot;\cdot)$	Incomplete Gamma function with lower regularization
25.	$Q(\cdot)$	Gaussian Q-function
26.	${}_1F_0(\cdot)$	Hypergeometric binomial function
27.	$Le[\cdot]$	Laplace expansion

Further, minimal equicorrelations are introduced to enhance MIMO output performance levels [10]. At receiver, the combiner unit (reverse of beamsteering operation) aids the short-range intended user to achieve sufficient power levels. The method of Maximal Ratio Combining (MRC) is used [10]. To achieve the decoded bit stream, demodulation is applied to the recovered symbols present in $r(t)$ [2]. Section VII of this paper presents a performance analysis of the equicorrelated MM wave system based on MIMO-MRC received SNR statistics.

B. MM WAVE SCENARIO CONSIDERATIONS

MM wave communications are typically "short range" because of extremely high transmission frequencies [5]. Such systems can be broadly classified as having both

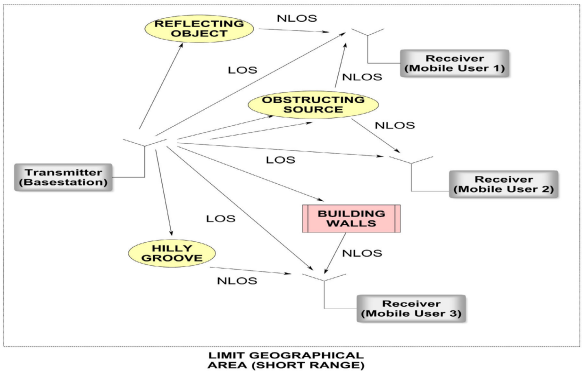

FIGURE 2. Short range LOS MM wave transmissions.

LOS and NLOS transmissions [12]. The MM wave channel statistics vary according to the transmission/reception mode chosen [9], [12]. The receiver may exist at two different user locations as follows.

- LOS user nearby to base-station (BS) [5].
- NLOS user nearby to BS [12].

Figure 2 depicts the transmissions at MM wave frequencies involving BS and close-LOS users [5]. In such situations, the receiver is assumed to be located near to the transmitter. The transmit-receive alignment primarily decides the strength of the signal received at the mobile station (MS) [4], [5], [13]. Steering the antenna in the desired user direction aids in achieving effective MM wave MIMO communications. If W is the weighing vector, $a(\theta)$ is the steering vector, and θ_d is the desired user angular location, beamsteering is accomplished by setting $W = a(\theta_d)$. MM wave transmissions for NLOS users in the proximity of BS can be visualized as similar to Figure 2 [9], [12]. However, the LOS paths between transmitter and receiver are blocked in such cases. Thus, received signal strength at MS depends on NLOS contributions. The beamsteering method was previously used under NLOS conditions with limited transmission distance [15], [16], [17].

A fully-digital MM wave MIMO communication model (that implements digitally beamsteered/beamformed transmission and MRC reception) with 2 phased arrays and a maximum of 2 antennas per array at the MS is considered under hardware constraints [77], [78]. On the other hand, the BS is assumed to have better design flexibility such that it can accommodate $m \geq 2$ antennas (more antennas than the MS). With m antennas at transmit BS and 2 antennas at receive MS, the proposed MM wave link ($m \times 2$ MIMO) is analyzed in the downlink scenario. Moreover, with 2 antennas at transmit MS and m antennas at receive BS, uplink analysis ($2 \times m$ MIMO) is carried out at MM wave frequencies [10], [12].

III. CORRELATED MM WAVE MIMO CHANNEL MODELING

This section deals with the modelling of correlation effects in a MM wave MIMO link [5] [10]. Initially, useful dependencies are derived from a typical MIMO channel at MM wave frequencies. Further, analytical MIMO models are utilized for introducing correlations into the considered MM wave channels. Thereafter, key statistical measures are evaluated from the obtained correlated MM wave MIMO. Different mathematical notations used in this paper along with their descriptions are listed in Table 1.

A. MIMO MODELING OF BEAMSPACE MM WAVE CHANNELS

An analytical model specifically applicable to MM wave channels is proposed in [5]. The same is utilized for the current work based upon beamspace virtual representation. The characterization is called "virtual" as it considers an arrangement with equally spaced valid arrival and departure angles (AoAs/AoDs) typical of beamsteered MM wave links. This is illustrated using Eq. (1) and is termed as the possible AoA/AoD "dictionary." [5], [16].

$$\begin{aligned} v_i &= i\Delta v \\ &= \frac{i}{N}, i = 0, 1, \cdots, N-1 \end{aligned} \tag{1}$$

where, v_i represent the possible spatial departure or arrival angles and Δv depicts the uniform spacing between them. Based upon Eq. (1) and considering a 2×2 order MIMO i.e. $N_T \times N_R$ model with $N_T = 2$ and $N_R = 2$, the corresponding MM wave Beamspace MIMO channel is illustrated in Eq. (2). The detailed derivation of Eq. (2) can be referred to in Appendix-A. The $N_T \times N_R$ MM wave channel has been represented in Eq. (2) considering 2×2 MIMO for the ease of deduction. However, the subsequent analysis carried out holds for arbitrary values of N_T and N_R.

$$\Rightarrow H_{MM} = \frac{1}{\sqrt{N_R N_T}} \begin{bmatrix} A & B \\ C & D \end{bmatrix} \tag{2}$$

where,

$$\begin{aligned} A &= a^*_{T_1}(\theta_0)a_{R_1}(\theta_0)h_{11} + a^*_{T_1}(\theta_0)a_{R_2}(\theta_0)h_{21} \\ &\quad + a^*_{T_2}(\theta_0)a_{R_1}(\theta_0)h_{12} + a^*_{T_2}(\theta_0)a_{R_2}(\theta_0)h_{22} \\ B &= a^*_{T_1}(\theta_1)a_{R_1}(\theta_0)h_{11} + a^*_{T_1}(\theta_1)a_{R_2}(\theta_0)h_{21} \\ &\quad + a^*_{T_2}(\theta_1)a_{R_1}(\theta_0)h_{12} + a^*_{T_2}(\theta_1)a_{R_2}(\theta_0)h_{22} \\ C &= a^*_{T_1}(\theta_0)a_{R_1}(\theta_1)h_{11} + a^*_{T_1}(\theta_0)a_{R_2}(\theta_1)h_{21} \\ &\quad + a^*_{T_2}(\theta_0)a_{R_1}(\theta_1)h_{12} + a^*_{T_2}(\theta_0)a_{R_2}(\theta_1)h_{22} \\ D &= a^*_{T_1}(\theta_1)a_{R_1}(\theta_1)h_{11} + a^*_{T_1}(\theta_1)a_{R_2}(\theta_1)h_{21} \\ &\quad + a^*_{T_2}(\theta_1)a_{R_1}(\theta_1)h_{12} + a^*_{T_2}(\theta_1)a_{R_2}(\theta_1)h_{22} \end{aligned}$$

It can be observed from eq. (2) that even with large number of MM wave BS antennas (m) as described in Section II-B (leading to increased transmitter antennas in downlink and increased receiver antennas in uplink), the channel complexity does not drastically increase with the matrix entries being limited to the four terms A, B, C and D, each of them being simple, linear combinations of transceiver steering vectors (at chosen AoD/AoA) and tap gains. The referred channel matrix so formed is computationally not very

intensive both in terms of generation and estimation. This makes it suitable for fully digital beamsteered/beamformed transmission and simplistic MRC based reception avoiding the use of more complex hybrid (analog-digital) precoding. Moreover, it is crucial to observe that MM wave channel taps are directly dependent on transceiver steering vectors [5]. There is indeed a necessity to analyze MIMO output statistics and receiver performance in terms of such tunable vectors to devise link performance improvements at MM wave frequencies [31], [32], [33], [34], [35].

B. DOUBLE CORRELATED MM WAVE MIMO MODEL

Analytical models popularly used for MIMO characterization are illustrated in [11]. From each of those, a separate correlation MIMO model was chosen to effectively analyze the NLOS MM wave channels for the following reasons: Firstly, it is selected to facilitate evaluation of MM wave statistics and reception parameters in terms of antenna correlations [7], [10]. Also, separately correlated models are utilized rather than combined correlation models because the latter is more computationally complex [11]. Furthermore, the double correlation model is easily applicable to MIMO communications, which use fewer scatterers at the transmit and receive terminals, reducing multipaths [5], [10]. Thus, it is ideal for applying to MM wave transmissions where higher frequency components result in reduced scattering and a corresponding lower number of multipaths [36], [37], [38], [39], [40]. Furthermore, the taps for the considered model are selectively Gaussian or Rayleigh, depicting LOS or NLOS MM wave characteristics [11], [12].

1) KRONECKER MODELING OF MM WAVE MIMO CHANNELS

The separately correlated model considers correlations individually between elements at the transmitter and also at the receiver due to space limitations [11]. However, due to sufficient separation, correlations at the transmitter and receiver are themselves independent [10].

Let H_{MM} be an $N_T \times N_R$ narrowband channel at MM wave frequencies, a special case of which is depicted in Eq. (2). The correlation matrices at transmit and receive sides are represented by $R_{TX_{MM}}$ and $R_{RX_{MM}}$ respectively. Therefore, the Kronecker product [$\bigotimes$] of independent terms $R_{TX_{MM}}$ and $R_{RX_{MM}}$ signifies the total correlation matrix mathematically [11]. It is shown in Eq. (3).

$$R_{H_{MM}} = E[h_{MM} h_{MM}^H] = R_{TX_{MM}}^T \bigotimes R_{RX_{MM}} \tag{3}$$

where, $h_{MM} = vect(H_{MM})$. The transmitter and receiver correlations are evaluated using Eqs. (4) and (5).

$$R_{TX_{MM}} = E\{[H_{MM}^H H_{MM}]^T\} \tag{4}$$

$$R_{RX_{MM}} = E[H_{MM} H_{MM}^H] \tag{5}$$

2) MIMO STATISTICS FOR DOUBLE CORRELATED MM WAVE CHANNELS

The illustrations in [10] and [11] reveal that for independent transmitter and receiver correlations, MM wave MIMO decomposition is readily obtained using Eq. (6).

$$H_{MM_{Kron}} = R_{RX_{MM}}^{\frac{1}{2}} H_R R_{TX_{MM}}^{\frac{1}{2}} \tag{6}$$

The entries of matrix H_R depend on relevant channel statistics. In the proposed work, the link is NLOS and therefore the MM wave taps will be Rayleigh. Further, $H_{MM_{Kron}}$ denotes a double correlation MM wave decomposed MIMO channel [11], [12]. Appendix-B describes the correlation fading statistics prevalent in MIMO systems.

Using Eqs. (2), (4) and (5) we can clearly infer that $R_{TX_{MM}}$ and $R_{RX_{MM}}$ depend on tunable steering vectors $a_T(\theta_T)$ and $a_R(\theta_R)$. Thus, through efficient tuning, transmit and receive correlation levels can be *adapted* [5], [11]. Moreover, using Eq. (3), the overall correlation $R_{H_{MM}}$ could therefore be similarly adjusted to decrease the overall correlation levels [8]. It holds true only for MM wave links but not microwave [5], [11].

This dependency is further ascertained while observing statistics of the generalized MM wave MIMO channel (H_{MM}), a special case of which is illustrated in Eq. (2). H_{MM} or equivalently h_{MM} consisting of $N_R \times N_T$ components can be characterized as a *zero mean* random vector with *covariance* signified by $R_{H_{MM}}$ i.e. $h_{MM} \sim \mathcal{N}_C^{N_R \times N_T}(0, R_{H_{MM}})$. The PDF for H_{MM} is further illustrated using Eq. (7). These analytical expressions are however applicable for links with LOS paths and such channel taps are therefore complex Gaussian [11]. In the studied literature, closed form analysis for PDF of MM wave correlated NLOS channels is not available [1], [2], [3], [4], [5], [6], [7], [8], [9], [10], [11], [12], [13], [14], [15], [16], [17], [18], [19], [20], [21], [22], [23], [24], [25], [26], [27], [28], [29], [30], [31], [32], [33], [34], [35], [36], [37], [38], [39], [40], [41], [42], [43], [44], [45], [46], [47], [48], [49], [50], [51], [52], [53], [54], [55], [56], [57], [58], [59], [60], [61], [62], [63], [64], [65], [66], [67], [68], [69], [70], [71], [72], [73], [74], [75], [76].

$$p(h_{MM}) = \frac{1}{(\pi)^{N_T N_R} det(R_{H_{MM}})} e^{-(h_{MM})^H R_{H_{MM}}^{-1} h_{MM}} \tag{7}$$

The PDF of H_{MM} therefore directly varies with the overall correlation, $R_{H_{MM}}$. This reveals that only in the MM wave regime, the link statistics and thereby the receiver output can be altered by tuning the steering/response vectors.

IV. BEAMSTEERED MM WAVE MIMO-MRC SYSTEM ANALYSIS

While channel statistics are key to linking baud measurements, analysis of MIMO receiver statistics is crucial in evaluating MM wave output performance. The bemasteered MM wave signal is received by the mobile device utilizing the MRC process [10] as described below [46], [47], [48], [49].

A. MRC RECEIVER MODEL FOR MM WAVE MIMO

Consider a model with N_T antennas at transmitter and N_R antennas at receiver. Therefore, the system input will be of size $N_T \times 1$, the channel matrix (H_{MM}) will be $N_R \times N_T$ in

dimension and the received output r has dimension $N_R \times 1$ [61]. The receiver output vector, r is expressed as in Eq. (8)

$$r = \sqrt{\overline{\gamma}} H_{MM} W x + n_g \tag{8}$$

where, x is the transmitted symbol with $E[x^2] = 1$, W denotes the weight vector for beamsteering such that $E[||W||^2] = 1$, $\overline{\gamma}$ represents input SNR, n_g is the complex noise of Gaussian nature modeled as $noise \sim \mathcal{CN}_{N_R,1}(O_{N_R \times 1}, I_{N_R})$. Moreover, H_{MM}, the NLOS (Rayleigh) MIMO matrix at MM wave frequencies is of dimension $N_R \times N_T$ [38], [50], [51], [52], [53].

Further, the H_{MM} matrix of Eq. (8) can be decomposed as described by Eq. (6). Upon splitting, Eq. (8) can be expressed using Eqs. (9) and (10).

$$r = \sqrt{\overline{\gamma}} H_{MM_{Kron}} W x + n_g \tag{9}$$

$$r = \sqrt{\overline{\gamma}} \{R_{RX_{MM}}^{\frac{1}{2}} H_R R_{TX_{MM}}^{\frac{1}{2}}\} W x + n_g \tag{10}$$

Eq. (10) clearly indicates that the signal received at the input of MRC (and output thereby) of the MIMO MM wave system depends on transceiver correlations [11]. Therefore, steering vector adjustment will lead to reduced transmit-receive correlations and, thus, will result in improved signal reception. H_R indicates Rayleigh (NLOS) channel taps [10]. Next, crucial performance metrics for MM wave MRC receivers are evaluated as a function of antenna correlations [10], [11], [54].

MRC receivers implement signal combining with maximal ratio and evaluate the combined output Z using Eqs. (11), (12), (13) as depicted in [9] and [11]. r is the MRC system input described by Eq. (8).

$$Z = W^{\dagger} H_{MM}^{\dagger} r \tag{11}$$

$$Z = W^{\dagger} H_{MM}^{\dagger} (\sqrt{\overline{\gamma}} H_{MM} W x + n_g) \tag{12}$$

$$Z = \sqrt{\overline{\gamma}} W^{\dagger} H_{MM}^{\dagger} H_{MM} W x + W^{\dagger} H_{MM}^{\dagger} n_g \tag{13}$$

$W^{\dagger}$ and W here represent the combining and beamsteering vectors respectively. $H_{MM}^{\dagger}$ denotes Hermitian estimate of the MM wave channel [10]. When we compare Eq. (8) with Eq. (13), the MRC output SNR can be expressed using Eq. (14)

$$\gamma = \overline{\gamma} W^{\dagger} H_{MM}^{\dagger} H_{MM} W \tag{14}$$

Utilizing Eq. (2), we can obtain Eq. (15) from Eq. (14) as below.

$$\gamma = \frac{1}{N_R N_T} \overline{\gamma} W^{\dagger} \begin{bmatrix} A & B \\ C & D \end{bmatrix}^{\dagger} \begin{bmatrix} A & B \\ C & D \end{bmatrix} W \tag{15}$$

where, A, B, C and D are matrix entries that are direct functions of tunable steering and response vectors $a_T(\theta_T)$ and $a_R(\theta_R)$ respectively. Thus, Eq. (15) shows that received SNR for a 2×2 MIMO-MRC arrangement at MM wave frequencies is dependent on steering/response vectors or corresponding AoDs/AoAs [58], [59], [60]. The same statement is readily extendible to an $N_T \times N_R$ model. Therefore, accurate tuning of such vectors should result in improved signal reception which needs to be examined further [10]. Some significant advantages of using the proposed Correlation based MM wave system over ZF/DFE based systems are: (i) due to Kronecker based channel representation which decomposes the taps in terms of path gains and transceiver steering vectors, the tedious task of channel estimation (involving inconsistent matrix inversion operation) can be avoided, (ii) in a similar manner, the time consuming task of training (for proper estimation) which involves careful selection of pilot signals and associated complexities can also be circumvented. The proposed system tuned according to steering angle/vector rather emphasizes on proper directional alignment (best AoD/AoA combination) for equally minimized correlations resulting in significant performance rise.

B. BEAMSTEERING FOR SHORT RANGE MM WAVE COMMUNICATIONS

The weight vector W of Eq. (15) is chosen so as to maximize the SNR output and thereby minimize the error rate [6], [7]. The vector optimized thereby, W_{opt} signifies the eigen vector corresponding to the maximum eigen mode for $H_{MM}^{\dagger} H_{MM}$ [10], [11]. When W is set to W_{opt}, we obtain peak eigen mode for $H_{MM}^{\dagger} H_{MM}$ denoted by λ_m. In such scenarios, the combiner output SNR is obtained using Eq. (16).

$$\gamma = \overline{\gamma} \lambda_m \tag{16}$$

The MRC output SNR γ in MM wave regime depends on the statistics of λ_m which signifies double correlated complex Wishart maximum eigen value for $H_{MM}^{\dagger} H_{MM}$. It is critical to note that for analyzing γ statistically, this eigen mode is utilized [12], [26]. In Eq. (15), the weight vector W is set as $a(\theta_d)$ to achieve beamsteering which ensures satisfactory received power levels for mobile users in BS proximity. With signal presence ensured, the proposed work stresses on realizing SER reductions through correlation control [5], [61], [62].

V. MM WAVE MIMO-MRC PERFORMANCE ANALYSIS UNDER SEPARATELY CORRELATED RAYLEIGH ENVIRONMENTS

The performance of MIMO-MRC is analyzed in the MM wave regime based on double correlated Rayleigh (NLOS) statistics presented in Appendix-C. Previously, output evaluation for MIMO-MRC was carried out only under uncorrelated and semi-correlated channels where antenna correlations either exist at one end of the link or do not exist at all [10], [12]. For the baseline work referred to in [10], SER expressions under uncorrelated MIMO channels were derived by considering $2 \times m$ and $m \times 2$ systems, which correspond to uplink and downlink communications, respectively. Similar limitation of two antennas on either the transmit or receive side, more generalized SER closed form expressions are deduced under double-correlated MIMO Rayleigh environments in [10]. The error analysis in [10] and also most of the other relevant works such as [12] are however

only for microwave environments. On the contrary, very few works report correlated MIMO-MRC performance under the MM wave regime. Transmit/receive correlation matrices only at MM wave frequencies depend on steering/response vectors (or departure/arrival angles), and it is therefore crucial to inspect MIMO performance under MM wave channels. Only with the same MS and BS antenna considerations same as in [10], generalized SER and asymptotic (high SNR) SER closed form expressions are evaluated here for MIMO-MRC model under MM wave double correlated Rayleigh (NLOS) environments [15] where the dependency of MM wave channel parameters on steering vectors/angles could be exploited to improve the system performance which is not possible in case of the microwave MIMO model presented in [10].

The analytical expressions presented here initially assume $N_R \geq N_T$ resulting in full rank $H_{MM}^{\dagger}H_{MM}$. Under such conditions, the model parameters are tuned as $\Omega = R_{Tx_{MM}}$, $\sum = R_{Rx_{MM}}$, $n = N_T$ and $m = N_R$. Subsequently, considering $N_R < N_T$, the maximum eigen value still remains the same leading to identical closed form expressions [10]. However, in the later case with $H_{MM}H_{MM}^{\dagger}$ being full rank, the system parameters will be $\Omega = R_{Rx_{MM}}$, $\sum = R_{Tx_{MM}}$, $n = N_R$ and $m = N_T$. The above two cases shall be detrimental while evaluating MM wave SER under different communication modes [10], [11].

A. MM WAVE AVERAGE SYMBOL ERROR RATE

Closed form expressions for average SER of MIMO-MRC under separately correlated MM wave NLOS links are presented here considering both $2 \times m$ (uplink) and $m \times 2$ (downlink) systems for different modulation schemes [10], [12]. The generalized closed form expression for average SER of MM wave MIMO-MRC system under separately correlated NLOS (Rayleigh) MM wave channels is shown in Eq. (17). Detailed Average SER derivation can be referred to in Appendix-D.

$$\begin{aligned}\left(P_{S,MM}\right)_{av} &= \frac{det(\Omega)ab\overline{\gamma}}{\Delta_2(\Omega)\Delta_m(\sum)}\sum_{p=1}^{m}\sum_{t=1,t\neq p}^{m}(-1)^{p+\phi(t)}(\sigma_p\sigma_t)^{m-1} \\ &\cdot \Delta_{m-2}(\sigma^{[p,t]}) \times \left(\tilde{\eta}\left(0,-\frac{1}{\overline{\gamma}b}\left(\frac{1}{\omega_2\sigma_p}+\frac{1}{\omega_1\sigma_t}\right)\right)\right. \\ &\left. -\sum_{l=0}^{m-1}\frac{1}{l!}\frac{\tilde{\eta}\left(l,-\frac{1}{\overline{\gamma}b\omega_2\sigma_p}\right)}{(2\overline{\gamma}b\omega_1\sigma_t)^l} - \sum_{l=0}^{m-1}\frac{1}{l!}\frac{\tilde{\eta}\left(l,-\frac{1}{\overline{\gamma}b\omega_1\sigma_t}\right)}{(2\overline{\gamma}b\omega_2\sigma_p)^l}\right)\end{aligned} \tag{17}$$

It is significant to observe in the analytical expressions illustrated by Eq. (17) that the MM wave average SER hugely relies upon the parameters Ω and Σ [43]. For MIMO transmissions considered, the mentioned terms equate to correlation matrices at transmitter or receiver i.e. $R_{Rx_{MM}}$ or $R_{Tx_{MM}}$ [10], [11]. Also, the elaborations in Section III-B reveal that MM wave MIMO correlation entries (not microwave correlations) depend on transmit-receive steering vectors i.e. $a_T(\theta_T)$ and $a_R(\theta_R)$ [5]. Therefore, the proposed work reduces MM wave correlation levels and thereby average SER levels through proper system vector tuning. Section VII-B presents numerical changes in MM wave MIMO-MRC SER with alterations in correlation metrics [42].

Further, it is significant to analyze the proposed average MM wave SER closed form expressions for minimally equicorrelated MIMO-MRC under different communication modes i.e. uplink and downlink. Firstly, we consider the uplink scenario with 2 number of transmit MS antennas and m number of receive BS antennas. Under such arrangements, we express the uplink average SER obtained from Eq. (17) with parameter settings: $\Omega = R_{Tx_{MM}}$, $\sum = R_{Rx_{MM}}$, $n = N_T$ and $m = N_R$ as below.

$$\begin{aligned}\left(P_{S,MM}\right)_{av,U} &= \frac{det(R_{Tx_{MM}})ab\overline{\gamma}}{\Delta_2(R_{Tx_{MM}})\Delta_{N_R}(R_{Rx_{MM}})}\sum_{p=1}^{N_R}\sum_{t=1,t\neq p}^{N_R}(-1)^{p+\phi(t)} \\ &\cdot (\sigma_p\sigma_t)^{N_R-1}\cdot\Delta_{N_R-2}(\sigma^{[p,t]}) \\ &\times\left(\tilde{\eta}\left(0,-\frac{1}{\overline{\gamma}b}\left(\frac{1}{\omega_2\sigma_p}+\frac{1}{\omega_1\sigma_t}\right)\right)\right. \\ &\left. -\sum_{l=0}^{N_R-1}\frac{1}{l!}\frac{\tilde{\eta}\left(l,-\frac{1}{\overline{\gamma}b\omega_2\sigma_p}\right)}{(2\overline{\gamma}b\omega_1\sigma_t)^l} - \sum_{l=0}^{N_R-1}\frac{1}{l!}\frac{\tilde{\eta}\left(l,-\frac{1}{\overline{\gamma}b\omega_1\sigma_t}\right)}{(2\overline{\gamma}b\omega_2\sigma_p)^l}\right)\end{aligned}$$

Next, we assume the downlink case with m number of transmit BS antennas and 2 number of receive MS antennas. Given these system arrangements, the downlink average SER expression deduced using Eq. (17) and model settings: $\Omega = R_{Rx_{MM}}$, $\sum = R_{Tx_{MM}}$, $n = N_R$ and $m = N_T$ is shown as follows.

$$\begin{aligned}\left(P_{S,MM}\right)_{av,D} &= \frac{det(R_{Rx_{MM}})ab\overline{\gamma}}{\Delta_2(R_{Rx_{MM}})\Delta_{N_T}(R_{Tx_{MM}})}\sum_{p=1}^{N_T}\sum_{t=1,t\neq p}^{N_T}(-1)^{p+\phi(t)} \\ &\cdot (\sigma_p\sigma_t)^{N_T-1}\cdot\Delta_{N_T-2}(\sigma^{[p,t]}) \\ &\times\left(\tilde{\eta}\left(0,-\frac{1}{\overline{\gamma}b}\left(\frac{1}{\omega_2\sigma_p}+\frac{1}{\omega_1\sigma_t}\right)\right)\right. \\ &\left. -\sum_{l=0}^{N_T-1}\frac{1}{l!}\frac{\tilde{\eta}\left(l,-\frac{1}{\overline{\gamma}b\omega_2\sigma_p}\right)}{(2\overline{\gamma}b\omega_1\sigma_t)^l} - \sum_{l=0}^{N_T-1}\frac{1}{l!}\frac{\tilde{\eta}\left(l,-\frac{1}{\overline{\gamma}b\omega_1\sigma_t}\right)}{(2\overline{\gamma}b\omega_2\sigma_p)^l}\right)\end{aligned}$$

B. ASYMPTOTIC (HIGH SNR) SER UNDER CORRELATED MM WAVE SCENARIOS

The generalized asymptotic (high SNR) SER closed form expression for MM wave MIMO-MRC model under double correlated Rayleigh (NLOS) conditions is represented using Eq. (18) [5], [10], [11]. The step-wise Asymptotic SER deduction is discussed in Appendix-E.

$$\left(P_{S,MM}\right)_{hi}^{\infty} = \frac{a(4m-1)!!\cdot\overline{\gamma}^{-2m}}{b^{2m}2^{2m+1}m!(m+1)!det(\Omega)^m det(\sum)^2} \tag{18}$$

From Eq. (18), it can be readily inferred that the maximum diversity order for separately correlated MM wave MIMO-MRC is $2m$. Further, utilizing the well-known Hadamard inequality (presented in Theorem 16.8.2 of reference [23] cited in our baseline model [10]) and also noting that diagonal elements of Ω and Σ are unity, the following can be readily inferred.

$$0 \leq det(\Omega) \leq 1 \tag{19}$$

$$0 \leq det(\Sigma) \leq 1 \tag{20}$$

In the case where Ω and Σ are identity matrices, the conditions represented by Eqs. (19) and (20) will comprise only of upper limit equalities [11]. However, in general, Eqs. (19) and (20) indicate fractional contributions from $det(\Omega)$ and $det(\Sigma)$ to the denominator of Eq. (18) at $\overline{\gamma} \rightarrow \infty$. This effect will tend to degrade the MM wave SER performance in the asymptotic (high SNR) regime [12]. Quite similar to the MM wave average SER presented in Section V-A, the asymptotic (high SNR) SER expressions are also a function of the transmit-receive correlation measures i.e. $R_{Rx_{MM}}$ and $R_{Tx_{MM}}$. Thus, fine tuning of correlation matrix entries is expected to adjust the fractional values of $det(\Omega)$ and $det(\Sigma)$ in such a manner that asymptotic (high SNR) SER levels are also acceptably low [5], [11]. MM wave correlation measures (unlike microwave) vary directly with transmit/receive steering vectors or departure/arrival angles, resulting in minimised asymptotic (high SNR) SER levels achieved using the proposed model through precise angular adjustments [43]. This will in turn lead to higher degrees of reliability for MM wave transmissions. Section VII-B emphasizes on computational verification of diminished $\left(P_{S,MM}\right)_{hi}^{\infty}$ levels with lesser inter-element correlations for the proposed model.

Further, it is significant to analyze the presented asymptotic (high SNR) MM wave SER closed form expressions for minimal equicorrelation MIMO-MRC under similar uplink and downlink scenarios. Firstly, we consider the uplink condition with 2 number of transmit MS antennas and m number of receive BS antennas. Given such a system model, we express the uplink asymptotic (high SNR) SER obtained from Eq. (18) with attribute settings: $\Omega = R_{Tx_{MM}}$, $\sum = R_{Rx_{MM}}$, $n = N_T$ and $m = N_R$ as follows.

$$\left(P_{S,MM}\right)_{hi,U}^{\infty} = \frac{a(4N_R-1)!! \cdot \overline{\gamma}^{-2N_R} det(R_{Rx_{MM}})^{-2}}{b^{2N_R} 2^{2N_R+1} N_R!(N_R+1)! det(R_{Tx_{MM}})^{N_R}}$$

Next, the downlink case is assumed with m number of transmit BS antennas and 2 number of receive MS antennas. With these model settings, the downlink asymptotic (high SNR) SER expression obtained using Eq. (18) and the parameter considerations: $\Omega = R_{Rx_{MM}}$, $\sum = R_{Tx_{MM}}$, $n = N_R$ and $m = N_T$ is illustrated as below.

$$\left(P_{S,MM}\right)_{hi,D}^{\infty} = \frac{a(4N_T-1)!! \cdot \overline{\gamma}^{-2N_T} det(R_{Tx_{MM}})^{-2}}{b^{2N_T} 2^{2N_T+1} N_T!(N_T+1)! det(R_{Rx_{MM}})^{N_T}}$$

VI. MM WAVE COMMUNICATIONS WITH MIMO EQUICORRELATIONS

In the proposed model, MIMO systems operating in the MM wave spectrum [5] are viewed under double-correlated scenarios utilizing [10], [11]. Using Eqs. (17) and (18), adequate control on key MM wave MIMO-MRC performance metrics (i.e., average and asymptotic (high SNR) SER) is achieved. The reception quality is proposed to be improved through effective tuning of correlation matrix entries [5], [11]. System level realization of the same is done by adjusting steering vectors or transmit-receive angles, which enables us to achieve the desired correlation measures. However, it is vital to infer the ideal entries of Kronecker correlation matrices for satisfactory MM wave MIMO performance. Transceiver vectors can be tuned accordingly to achieve the same. To start with, analytical correlation models for enhanced reception at MM wave frequencies are described [11], [15]. Next, to validate such performance gains, practical correlation models are utilized in the current work [43].

A. EQUICORRELATED KRONECKER MODEL

Based on the illustrations in [11], the transceiver matrices for antenna correlations in NLOS MM wave links are represented using Eqs. (21) and (22) for a 2×2 MIMO. However the obtained matrices are readily extendible to an $N_T \times N_R$ case.

$$R_{Tx_{MM}} = \begin{bmatrix} 1 & \rho_T & \rho_T & \rho_T \\ \rho_T & 1 & \rho_T & \rho_T \\ \rho_T & \rho_T & 1 & \rho_T \\ \rho_T & \rho_T & \rho_T & 1 \end{bmatrix} \tag{21}$$

$$R_{Rx_{MM}} = \begin{bmatrix} 1 & \rho_R & \rho_R & \rho_R \\ \rho_R & 1 & \rho_R & \rho_R \\ \rho_R & \rho_R & 1 & \rho_R \\ \rho_R & \rho_R & \rho_R & 1 \end{bmatrix} \tag{22}$$

with ρ_T and ρ_R indicating the transmit-receive correlation co-efficients respectively. They quantify the inter-antenna correlation levels limiting transceiver operations [11]. Specifically, for $\rho_T = \rho_R = \rho$ and using Eqs. (21) and (22), we express Eq. (23) as follows.

$$R_{Tx_{MM}} = R_{Rx_{MM}} = \begin{bmatrix} 1 & \rho & \rho & \rho \\ \rho & 1 & \rho & \rho \\ \rho & \rho & 1 & \rho \\ \rho & \rho & \rho & 1 \end{bmatrix} \tag{23}$$

When the MIMO NLOS link is represented using the same correlation matrix at transmit and receive side, the resulting channel model is an equicorrelated MM wave MIMO [11], [12]. Antenna correlations are solely described by the correlation coefficient (ρ). Higher is the ρ value, more is the correlation and thereby limit link performance [11]. Typically, ρ assumes values such as 0.1, 0.3, 0.5, 0.6, 0.7, 0.9 etc. The ideally desired uncorrelated case is reflected when $\rho = 0$. In the MM wave regime, transmit and receive antennas are steered using the minimal correlation arrival/departure vector [12]. Also, the suitable vector or

transmit-receive angle is selected from a possible departure/arrival angle dictionary [5]. A desired ρ value i.e. ρ_{tar} which leads to minimal antenna correlations is utilized for the proposed work [7]. ρ_{tar} value should be as minimum as possible. Thus, for performance gains under correlated MM wave channels, it is further suggested to model a minimal equicorrelation MIMO system. Average SER and asymptotic (high SNR) SER are analyzed for minimally equicorrelated links by incorporating the principle of Eq. (23) into Eqs. (17) and (18), respectively [5], [11]. Reduced equicorrelations lead to lowered MM wave SER levels under short-range NLOS scenarios [12].

B. ANGULAR VARIANCE BASED MINIMAL EQUICORRELATIONS IN MM WAVE MIMO-MRC SYSTEMS

In the proposed work, although the analytical modelling to achieve MIMO equicorrelations in MM wave systems is devised from the elaborations put forward in Section VI-A, the experimental inferences are drawn using a practical transceiver spread based correlation model illustrated in [10]. The numerical expressions consider Uniform Linear Arrays (ULAs) to exist both on the transmit and receive sides. Moreover, we assume subsequent element spacing (calculated in number of wavelengths) to be d_r and d_t at reception and transmission end respectively. Also, we consider θ_t and θ_r as the mean transmit AoD and receive AoA respectively. σ_t^2 and σ_r^2 are the transmit and receive angular spreads about mean AoD and AoA. Thereby, the adjusted transmitter AoD/receiver AoA is expressed using Eqs. (24) and (25).

$$\theta_{t_{mod}} = \theta_t + \hat{\theta}_t \tag{24}$$

$$\theta_{r_{mod}} = \theta_r + \hat{\theta}_r \tag{25}$$

with $\hat{\theta}_t \sim \mathcal{N}(0, \sigma_t^2)$ and $\hat{\theta}_r \sim \mathcal{N}(0, \sigma_r^2)$ representing the change in AoD and AoA respectively due to MM wave antenna tuning. Practical realization of the same shall be achieved by utilizing tunable 5G hardware proposed for future wireless communications [5], [10]. In this regard, the $(p, q)^{th}$ element of MM wave correlation matrices incorporating angular variances at transmit-receive sides is deduced as elaborated in Appendix-B and is represented using Eqs. (26) and (27).

$$(R_{Tx_{MM}})_{p,q} = e^{-j2\pi(p-q)d_t\cos(\theta_t)} e^{-0.5(2\pi(p-q)d_t\sin(\theta_t)\sigma_t)^2} \tag{26}$$

$$(R_{Rx_{MM}})_{p,q} = e^{-j2\pi(q-p)d_r\cos(\theta_r)} e^{-0.5(2\pi(q-p)d_r\sin(\theta_r)\sigma_r)^2} \tag{27}$$

While applying angular correlation spreads into the MIMO link at MM wave frequencies, similar departure and arrival angle mean values i.e. θ_t and θ_r are chosen from the MM wave pre-fixed dictionary (elaborated in Section III-A) so that the transmit and receive antennas are directed towards each other. For the proposed short range transmissions, beamsteering is incorporated [5], [10]. Further, in Eqs. (26) and (27), the transceiver variances σ_t^2 and σ_r^2 are set equally to achieve MM wave MIMO equicorrelations [11]. Also, it can be easily inferred using Eqs. (24) and (25) that for higher spreads i.e. σ_t^2/ σ_r^2, the departure/arrival angle variations i.e. $\hat{\theta}_t$ / $\hat{\theta}_r$ will also be higher. Thus, signals are transmitted by different antennas at well separated angles, leading to fewer correlations. Oppositely, with lower variances, the spreads will be less, leading to similar transmit-receive angles and thus increased correlations. Hence, for improved reception (i.e., minimal SER levels), the transmitter and receiver variance values are set to be maximally equal. It is in accordance with the concepts put forward in Section VI-A where MM wave performance improvement is suggested through minimally equicorrelated MIMO modelling [11]. System level realization of proposed minimal equicorrelations is achieved by adjusting the departure and arrival angles (or steering vectors) as per Eqs. (24) and (25) using tunable 5G antennas [5].

TABLE 2. Simulation Parameters.

S.No.	Parameter	Setting
1.	Communication model	MM wave MIMO-MRC
2.	Performance measures	Average SER, asymptotic (high SNR) SER
3.	User Location	Short range, NLOS
4.	Carrier Frequency	28 GHz, 32 GHz, 60 GHz and 72 GHz
5.	Mode of Communication	Uplink ($2 \times m$), Downlink ($m \times 2$)
6.	Limitation on number of antennas	Maximum 2 at transmitter (uplink), maximum 2 at receiver (downlink)
7.	Number of BS antennas (m)	2, 3, 4, 5, 8, 10, 12, 15, 20 and upto 256
8.	Inter-antenna spacing	$\frac{\lambda}{2}$
9.	Relative antenna gap (d_t, d_r)	0.5
10.	Antenna directivity	Beamsteering
11.	Mean AoD and AoA (θ_t, θ_r)	$\frac{\pi}{2}$
12.	Transceiver angular variances ($\sigma^2_{t/r}$)	$\frac{\pi}{8}$, $\frac{\pi}{14}$, $\frac{\pi}{15}$, $\frac{\pi}{16}$ (low correlations), $\frac{\pi}{20}$, $\frac{\pi}{22}$, $\frac{\pi}{32}$ (medium correlations), $\frac{\pi}{40}$, $\frac{\pi}{45}$ and $\frac{\pi}{64}$ (high correlations)
13.	Input SNR ($\overline{\gamma}$)	-20 to 50 dB
14.	Modulation format	4-PAM, BFSK-MC, BFSK-OS, BPSK and QPSK

VII. EXPERIMENTAL OBSERVATIONS

Depending on the proposed system, MM wave MRC reception of the minimal equicorrelation MIMO model [5], [11], [43] is studied under Rayleigh fading scenarios. Initially, the simulation settings considered are discussed. Next, the performance analysis of the MM wave MIMO-MRC system is showcased under equicorrelated NLOS environments.

A. PARAMETER SETTINGS

Table 2 illustrates the different simulation parameters used for the proposed work alongwith their default values.

Simulation Methodology. Standard procedures similar to those stated in [64] have been adopted for the simulation

process carried out using *MATLAB R2021a (9.10)* in this paper. Only a glimpse of the entire procedure carried out is presented here. MM wave SER simulations for MIMO-MRC are performed using adequate number of variables corresponding to crucial system parameters discussed above. "SNR_{in}" and "$SNRi_{mag}$" are vectors which define SNR in dB and magnitude terms with the former considered in the range of around -20 dB to 50 dB. To compute average SER over the specified SNR range, the code fragment for *se* computation is simulated over "$length(SNR_{in})$" iterations. Transceiver correlation variables, S and R are individually computed considering nested "*for*" loop structures with each loop run till respective MIMO dimension. The SER simulations in the paper are carried out considering a parametric model consisting of two matrices "*omg*" and "*sig*" whose eigen values are computed using built-in "*eig*" function and their m^{th} / 2^{nd} order Vandermonde determinants are computed using *nested for-while* loop structures with maximum of m iterations. The normalized complex multivariate Gamma variable "*gam*" is practically evaluated using an n iteration *for* loop. The MM wave average SER in Eq. (17) consists of six (06) number of contributing sub-terms. Only linear operations are used to simulate the first sub-term. Nested m iteration for loops with inner if-else statements simulate the second sub-term. The third sub-term involves computing $(m-2)^{th}$ Vandermonde determinant upon eigen values followed by $m-2$ iteration nested *for-while* structure. The fourth sub-term in its first part involves *nested if-else* structures whereas its second part involves a $2m-1$ iteration *for* loop with embedded *nested if-else*. The difference between the two parts yields the final value of the sub-term. Similarly, the fifth sub-term in its first part involves an $m-1$ iteration *for* loop with embedded *nested if-else* structure whereas its second part involves a $2m-1$ iteration *for* loop with embedded *nested if-else*. The final value of the sub-term is computed as a $2m-1$ iterative difference between both parts. The computation carried out for the sixth sub-term is exactly identical to that of the fifth sub-term. A random stream of as high as 10^{75} bits is transmitted under different modulation schemes defined using variables a and b. To ensure minimal processing delays while simulating higher number of bits/symbols, *Batch Parallelization* method is applied to an *Intel Core i5*, *Quad Core*, 8 GB (RAM), 64-bit, 2.4 GHz system on which the proposed MM wave model is tested. Out of *four*, *three* active cores simultaneously process the large number of received bits/symbols in smaller groups whereas the *fourth* core is used for bit/symbol allocation to a particular core prior to processing. The *Parallel Processing Toolbox* of *MATLAB* is utilized to achieve the same. Also, the steep decrease in final SER values computed through a linear, non-iterative sequence of operations on all six sub-terms is effectively visualised using the *Multiple Precision Toolbox* of *MATLAB*. Similar strategies are used to simulate MM wave asymptotic (high SNR) SER represented using Eq. (18).

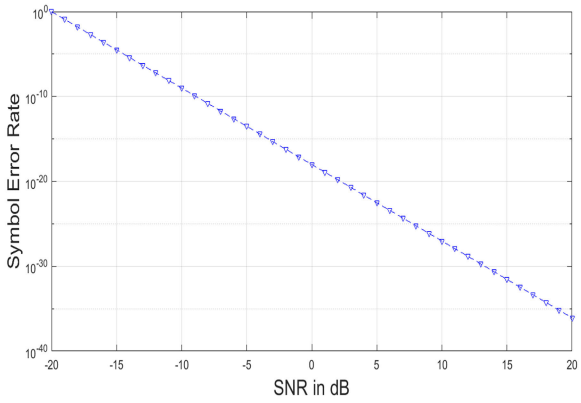

FIGURE 3. Uplink SER for Equicorrelated 2 × 10 MM wave MIMO-MRC under BPSK (Medium Corr. $\sigma^2_{t/r} = \frac{\pi}{32}$).

B. RESULTS AND ANALYSIS

Different results pertinent to equicorrelated MM wave MIMO-MRC output analysis under Rayleigh channels are categorized as below.

- Uplink SER analysis.
- Downlink SER analysis.
- Uplink asymptotic (high SNR) SER analysis.
- Downlink asymptotic (high SNR) SER analysis.
- Comparison and Significance of Minimally Equicorrelated Model versus Existing Models.

Detailed analysis on each of the above categories is as follows.

1) UPLINK SER ANALYSIS

Average SER for MM wave MIMO-MRC system is initially analyzed for uplink $2 \times m$ communications under separately correlated Rayleigh (NLOS) environments. Considering Eq. (17), MM wave SER is simulated and then observed with variations only in input SNR levels, $\overline{\gamma}$. Furthermore, the error rates are then inspected by additionally changing the correlation levels, MIMO order, and modulation schemes.

Firstly, average SER for the proposed equicorrelated MIMO-MRC model is evaluated under NLOS MM wave scenarios considering a fixed correlation level ($\sigma^2_{t/r}$), particular modulation format and specific MIMO order. Figure 3 illustrates uplink SER for a 2×10 MM wave MIMO-MRC system with medium equicorrelations of $\sigma^2_{t/r} = \frac{\pi}{32}$ and BPSK modulation. With increasing levels of input SNR (in dB), the symbol error is observed to reduce. The average SER curves simulated for input SNR, with $\overline{\gamma}$ set between -20 dB and 50 dB, agree with established theory and also with the utilised mathematical framework [5], [11], [43].

Next, the proposed equicorrelated MM wave model is analyzed for varying correlation levels ($\sigma^2_{t/r}$). Each representative case considers a particular MIMO configuration and a specific modulation technique. However, the observations are recorded for multiple MIMO orders and different modulation modes [12].

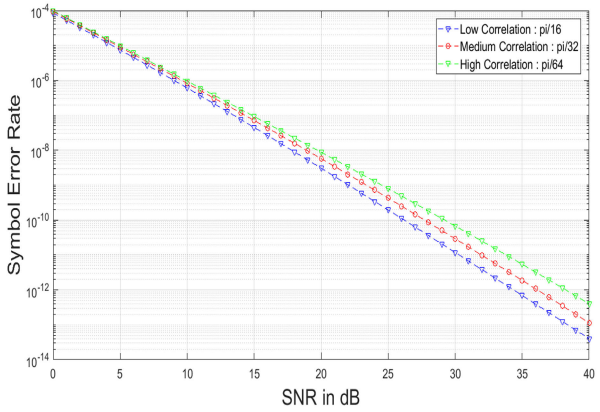

FIGURE 4. Variation of BPSK Uplink SER for Equicorrelated 2 × 3 MM wave MIMO-MRC with correlation levels.

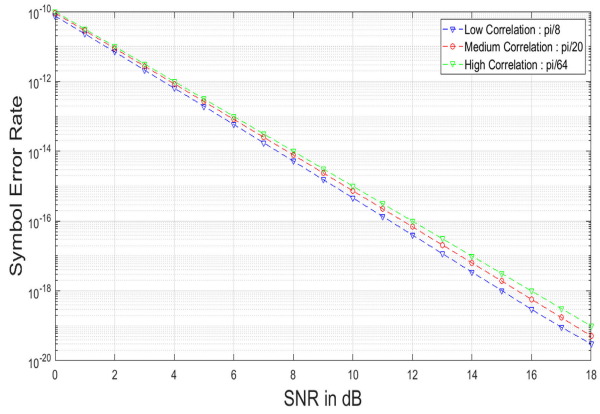

FIGURE 5. Variation of BPSK Uplink SER for Equicorrelated 2 × 6 MM wave MIMO-MRC with correlation levels.

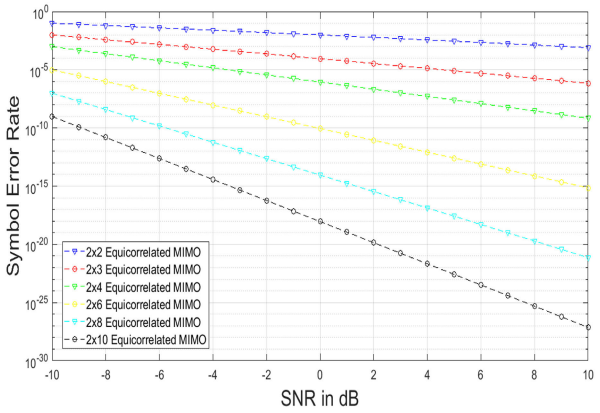

FIGURE 6. Uplink BFSK-MC SER for Equicorrelated MM wave system with different MIMO orders (Low Corr. $\sigma^2_{t/r} = \frac{\pi}{16}$).

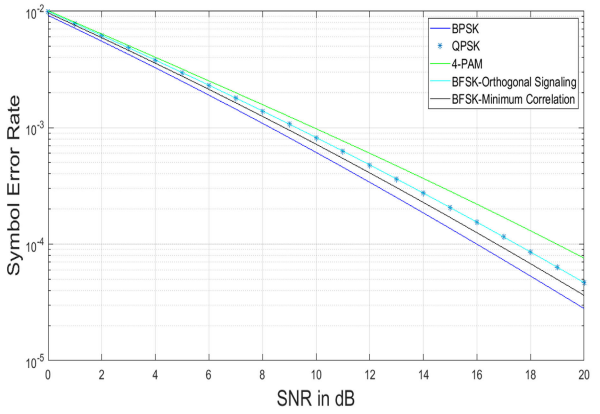

FIGURE 7. Uplink SER for 2 × 12 Equicorrelated MM wave MIMO with different modulation schemes (Low Corr. $\sigma^2_{t/r} = \frac{\pi}{8}$).

Figure 4 compares average SERs for the proposed NLOS model with MIMO order 2×3 under low ($\sigma^2_{t/r} = \frac{\pi}{16}$), medium ($\sigma^2_{t/r} = \frac{\pi}{32}$) and high correlation ($\sigma^2_{t/r} = \frac{\pi}{64}$) levels. The communication mode is uplink and the modulation format used is BPSK [10]. It can be clearly seen from Figure 4 that with lower antenna equicorrelations (or higher angular variances), the average SER levels at MM wave MRC output are lower.

Moreover, it is observed in Figure 5 that with increasing number of BS antennas i.e. $m = 6$, the difference in error levels for high and medium correlations are not that prominent. This is due to the fact that with more BS antennas, the overall received signal strength (or chance of weak faded path) is more resulting in similar error rates for high ($\sigma^2_{t/r} = \frac{\pi}{64}$) and medium ($\sigma^2_{t/r} = \frac{\pi}{20}$) correlations. However, for significantly low correlations i.e. ($\sigma^2_{t/r} = \frac{\pi}{8}$), even with more antennas, the average SER levels are prominently lesser as compared to those for high correlations ($\sigma^2_{t/r} = \frac{\pi}{64}$). Therefore, the current work achieves minimal equicorrelations through tuned AoAs and AoDs (or steering vectors) and thereby SER reductions in the MM wave MIMO uplink.

Further, performance of the proposed MM wave equicorrelation based model is examined by varying the number of BS antennas, m. The number of antennas is varied as 2,3,4,6,8 and 10. The performance is evaluated in terms of a specific correlation level $\sigma^2_{t/r}$ as well as a specific modulation scheme. The same study is however conducted by altering the correlation levels and also the modulation formats [12].

Figure 6 depicts MM wave MIMO SER variations with different BS antennas (m) under low equicorrelations of $\sigma^2_{t/r} = \frac{\pi}{16}$ and assuming BFSK-MC modulation [12]. It is observed that with increase in number of antennas (m), the average SER for the equicorrelated MM wave MIMO is reduced in the uplink. This is because with more number of receive antennas, the signal strength at the receiver (BS) is expected to increase (more probability of weak fade path and so lesser error). The current state of 5G and future generation wireless technologies enables powerful BS designs with flexibility to accommodate more antennas. Following this, the MM wave performance achieved at a particular correlation level and with fewer antennas can be improved by deploying more antennas at the BS [5].

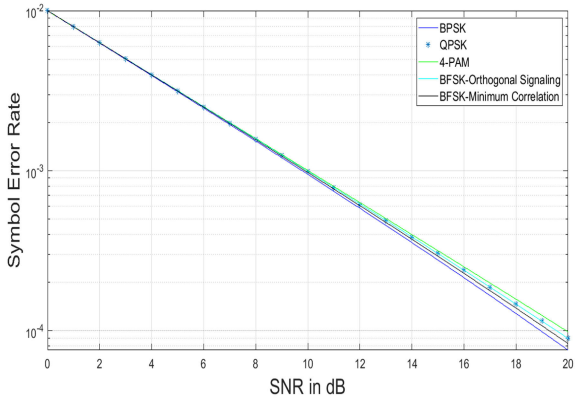

FIGURE 8. Uplink SER for 2 × 12 Equicorrelated MM wave MIMO with different modulation schemes (High Corr. $\sigma^2_{t/r} = \frac{\pi}{64}$).

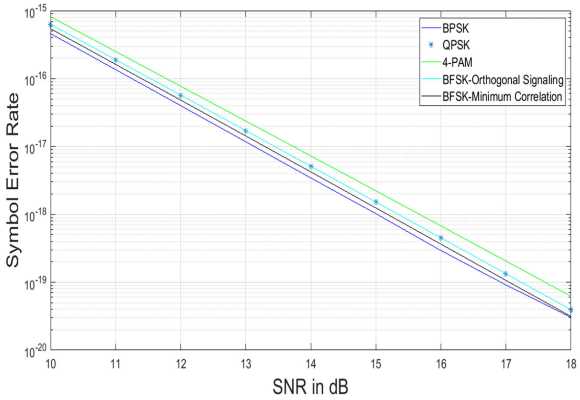

FIGURE 9. Uplink SER for 2 × 6 Equicorrelated MM wave MIMO with different modulation schemes (Low Corr. $\sigma^2_{t/r} = \frac{\pi}{8}$).

In addition, the proposed model is also comparatively analyzed in the uplink MM wave scenario for various modulation schemes [10], [11]. The study assumes a fixed correlation level $\sigma^2_{t/r}$ and specific MIMO order. Different representative cases of prevailing correlations and MIMO sizes are however considered for the analysis.

Figure 7 describes 2 × 12 MM wave system performance under different modulation schemes considering lower correlations $\sigma^2_{t/r} = \frac{\pi}{8}$. It can clearly be observed that the MM wave system provides least BER with BPSK. The SER with 4-PAM technique is observed to be on the higher side. For BFSK scheme, the performance is better than 4-PAM in general. Specifically, BFSK-MC system exhibits better SER performance as compared to BFSK-OS system due to inherently reduced impact of correlation. Further, with higher order PSK systems, i.e. QPSK, the performance is better than amplitude modulated systems (4-PAM). However, it shows higher SERs as compared to the BPSK system. Also, it is worthwhile noting that the BFSK-OS system has identical performance with respect to the QPSK model while the BFSK-MC link performs better than the higher-order QPSK system [5], [10].

Figure 8 represents average SER levels for the same 2 × 12 equicorrelated MIMO but under higher correlation effects i.e. $\sigma^2_{t/r} = \frac{\pi}{64}$. With increased correlations, otherwise satisfactorily performing BPSK versions of the proposed system show degraded SER. In such situations, BPSK and QPSK schemes are observed to have similar SER levels. More input SNR is therefore needed to yield lower SER with BPSK than that with QPSK under high correlation scenarios [11]. In such conditions, MM wave links assisted by lower SER techniques (such as BPSK) underperform as compared to systems built around higher SER schemes (i.e. BFSK-MC, BFSK-OS, QPSK).

In Figure 9, it can be observed that with lower correlations ($\sigma^2_{t/r} = \frac{\pi}{8}$) and higher number of BS antennas i.e. $m = 6$, the MM wave MIMO link with BFSK-MC modulation achieves SER levels similar to those obtained using BPSK method. The stated trends are prominent at a high SNR of around 18 dB.

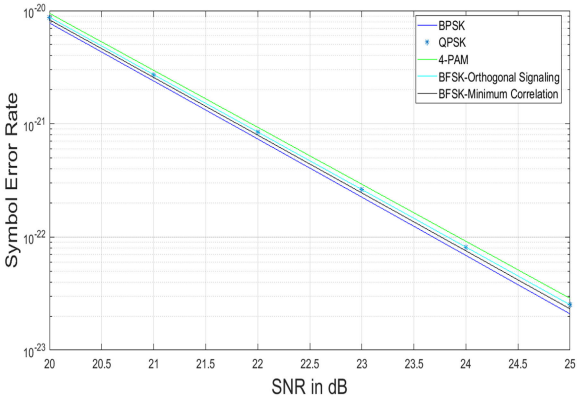

FIGURE 10. Uplink SER for 2 × 6 Equicorrelated MM wave MIMO with different modulation schemes (Med Corr. $\sigma^2_{t/r} = \frac{\pi}{32}$).

However, Figure 10 shows that with comparatively higher correlations ($\sigma^2_{t/r} = \frac{\pi}{32}$) and same m value, the BPSK system performance dominates that of BFSK-MC.

2) DOWNLINK SER ANALYSIS

Average SER for MM wave MIMO-MRC system is also analyzed in downlink $m \times 2$ communications under separately correlated Rayleigh (NLOS) environments. Considering Eq. (17), MM wave SER is simulated and then observed with variations only in input SNR levels, $\overline{\gamma}$. Furthermore, the error rates are then inspected by additionally changing the correlation levels, MIMO order, and modulation schemes. Table 3 accordingly summarizes the downlink average SER performance of the proposed model through comparisons with various scenarios during uplink.

Additionally, in Figure 11, it can be observed that with lower correlations ($\sigma^2_{t/r} = \frac{\pi}{8}$) and higher number of BS antennas i.e. $m = 6$, the MM wave MIMO link with BFSK-MC modulation achieves SER levels similar to those obtained using BPSK method. The stated trends are prominent at a high SNR of around 18 dB. However, Figure 12 shows that with comparatively higher correlations

TABLE 3. Downlink average and asymptotic (High SNR) SER.

S.No.	Analysis settings and type	MM wave SER trends
1.	Average SER, 8 × 2 MIMO, BFSK-OS, Low Corr. ($\sigma^2_{t/r} = \frac{\pi}{16}$)	Similar to that of Figure 3 in Section VII-B1 (Uplink SER Analysis)
2.	Average SER, 15 × 2 MIMO, 4-PAM, variation with correlation levels	Similar to that of Figure 4 in Section VII-B1 (Uplink SER Analysis)
3.	Average SER, 20 × 2 MIMO, BFSK-MC, variation with correlation levels	Similar to that of Figure 5 in Section VII-B1 (Uplink SER Analysis)
4.	Average SER, QPSK, Medium Corr. ($\sigma^2_{t/r} = \frac{\pi}{32}$), variation with MIMO order	Similar to that of Figure 6 in Section VII-B1 (Uplink SER Analysis)
5.	Average SER, 9 × 2 MIMO, Low Corr. ($\sigma^2_{t/r} = \frac{\pi}{16}$), variation with modulation schemes	Similar to that of Figure 7 in Section VII-B1 (Uplink SER Analysis)
6.	Average SER, 9 × 2 MIMO, High Corr. ($\sigma^2_{t/r} = \frac{\pi}{64}$), variation with modulation schemes	Similar to that of Figure 8 in Section VII-B1 (Uplink SER Analysis)
7.	Average SER, 6 × 2 MIMO, Low Corr. ($\sigma^2_{t/r} = \frac{\pi}{8}$) and More Corr. ($\sigma^2_{t/r} = \frac{\pi}{16}$) variation with modulation schemes	Similar to that of Figures 9,10 in Section VII-B1 (Uplink SER Analysis)
8.	Average vs Asymptotic SER, 8 × 2 MIMO, BFSK-MC, Low Corr. ($\sigma^2_{t/r} = \frac{\pi}{16}$)	Similar to that of Figure 15 in Section VII-B3 (Uplink Asymptotic (High SNR) SER Analysis)
9.	Average vs Asymptotic SER, 20 × 2 MIMO, BFSK-MC, Low Corr. ($\sigma^2_{t/r} = \frac{\pi}{16}$)	Similar to that of Figure 16 in Section VII-B3 (Uplink Asymptotic (High SNR) SER Analysis)

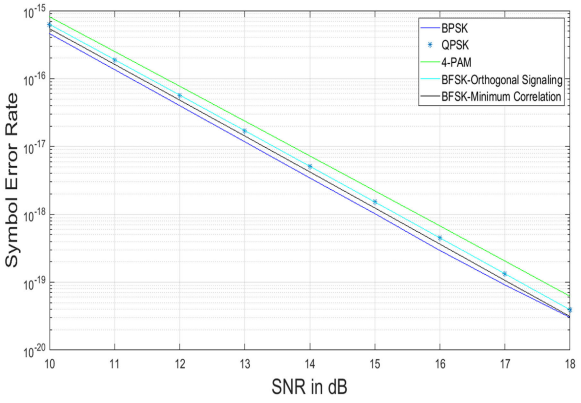

FIGURE 11. Downlink SER for 6 × 2 Equicorrelated MM wave MIMO with different modulation schemes (Low Corr. $\sigma^2_{t/r} = \frac{\pi}{8}$).

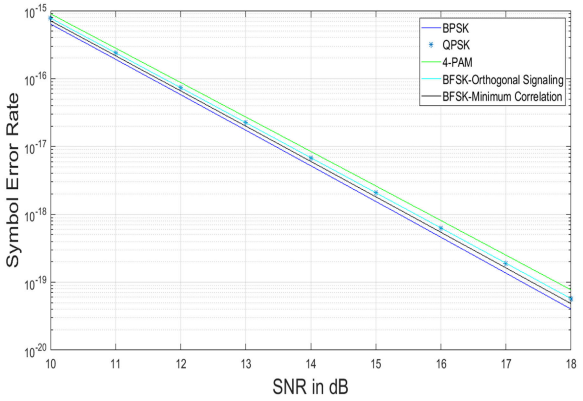

FIGURE 12. Downlink SER for 6 × 2 Equicorrelated MM wave MIMO with different modulation schemes (More Corr. $\sigma^2_{t/r} = \frac{\pi}{16}$).

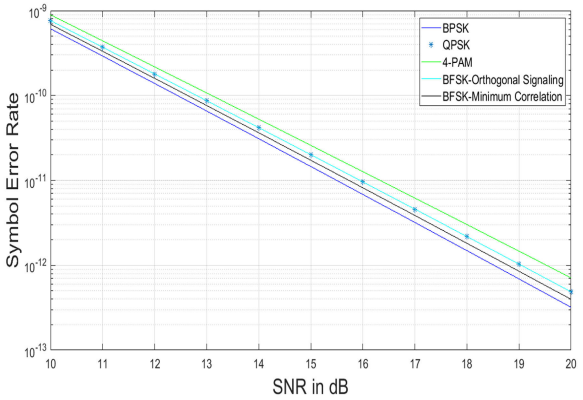

FIGURE 13. Uplink SER for 2 × 4 Equicorrelated MM wave MIMO with different modulation schemes (Low Corr. $\sigma^2_{t/r} = \frac{\pi}{16}$).

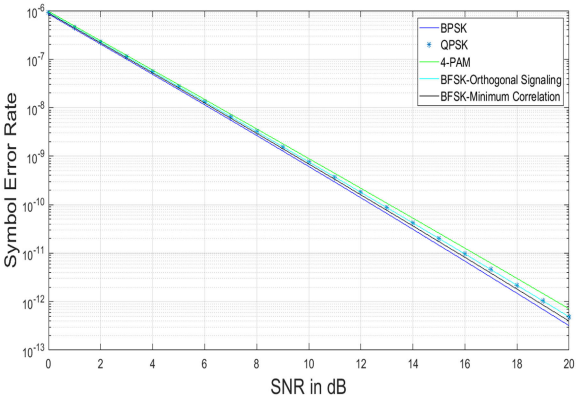

FIGURE 14. Downlink SER for 4 × 2 Equicorrelated MM wave MIMO with different modulation schemes (Low Corr. $\sigma^2_{t/r} = \frac{\pi}{16}$).

($\sigma^2_{t/r} = \frac{\pi}{16}$) and same m value, the BPSK system performance dominates that of BFSK-MC for the same range of input SNR.

Furthermore, the downlink and uplink MM wave performances are comparatively analyzed for various modulation formats. The study is conducted considering a particular MIMO order and specific correlation level ($\sigma^2_{t/r}$). However, the observations are validated for different representative correlation variances and MIMO configurations [11].

In comparison with the uplink average SERs depicted for proposed equicorrelated MIMO in Figure 13, the downlink SER levels for different modulation techniques are found to

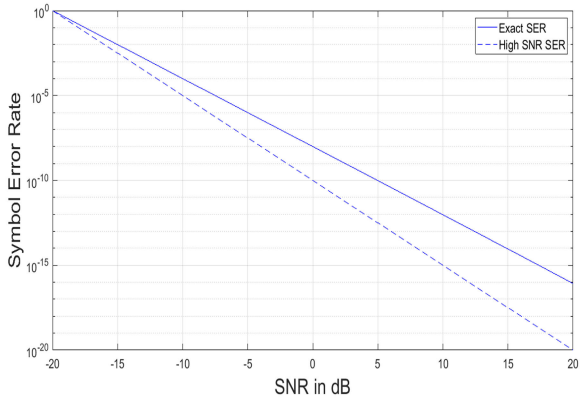

FIGURE 15. Average and Asymptotic (High SNR) SER comparison for Uplink 2 × 5 QPSK Equicorrelated MM wave MIMO (Med Corr. $\sigma^2_{t/r} = \frac{\pi}{32}$).

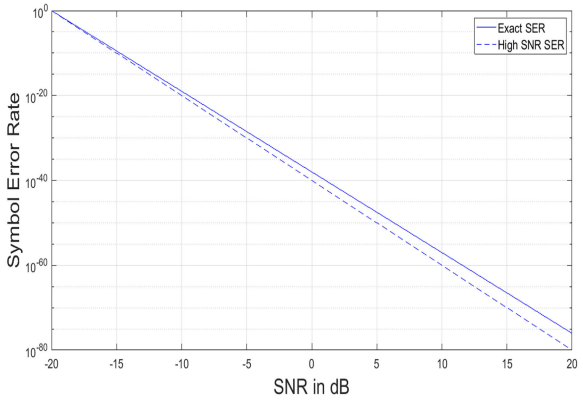

FIGURE 16. Average and Asymptotic (High SNR) SER comparison for Uplink 2 × 20 QPSK Equicorrelated MM wave MIMO (Med Corr. $\sigma^2_{t/r} = \frac{\pi}{32}$).

be quite similar as showcased in Figure 14. Here, we consider uplink and downlink cases both with 4 BS antennas and low correlations (i.e. $m = 4$ and $\sigma^2_{t/r} = \frac{\pi}{16}$). For downlink scenarios, with m copies being transmitted from BS and 2 copies received at MS, the signal strength per receive antenna is more leading to better performance for all modulation schemes. Thus, the gap between SERs corresponding to different modulation schemes is lesser. On the contrary, for uplink cases, only 2 copies are sent from MS with m copies received at BS. So, per receive antenna, the effective signal strength is lesser leading to inferior SER performance for all schemes. In such situations, the inherent efficiency of different modulation schemes determines the respective SER levels achieved (i.e., BPSK performs drastically better than 4-PAM or QPSK). The inferences made can be clearly observed through the separation between SER levels for various modulation schemes in uplink and downlink cases illustrated by Figures 13 and 14 respectively.

3) UPLINK ASYMPTOTIC (HIGH SNR) SER ANALYSIS

Next, asymptotic (high SNR) SER for MM wave MIMO-MRC link is evaluated for uplink $2 \times m$ systems under separately correlated Rayleigh environments. Using Eq. (18), MM wave SER (in asymptotic (high SNR) regime) is simulated and then observed with variations only in input SNR levels, $\overline{\gamma}$ for a fixed correlation level, specific modulation scheme and particular MIMO order. For practical demonstration of the asymptotic (high SNR) system behavior, finitely large input SNR values ranging upto as high as 20-30 dB are taken into account. Under such considerations, the asymptotic (high SNR) SERs obtained are compared with the average SERs evaluated from Eq. (17). Different representative cases by altering correlation levels, MIMO configurations, and modulation formats are observed to validate the study [15].

Figure 15 illustrates average and asymptotic (high SNR) SER comparisons in uplink scenarios for 2×5 equicorrelated MM wave MIMO under medium correlations $\sigma^2_{t/r} = \frac{\pi}{32}$ and considering QPSK modulated symbols. With lower number of BS antennas i.e. $m = 5$, it is observed that the asymptotic (high SNR) SER and average SER levels highly differ. This is because for the asymptotic (high SNR) case, SER is primarily a function of the input SNR and varies as $\overline{\gamma}^{-2m}$. As such, it shows significant decrease in error levels. However, in such cases, the crucial independent impact of eigen values for Ω and Σ i.e. $\omega_1, \omega_2, \cdots \omega_n$ and $\sigma_1, \sigma_2, \cdots \sigma_m$ are not taken into account. Only the direct effects of Ω and Σ are considered [11]. But, for average SER simulated using Eq. (17), the effect of these additional parameters are also considered and thus it models MM wave correlated channel behavior in a better manner. Therefore, with lower m values, the MIMO gains achieved in practice are not so high. This leads to increased average SER levels for higher input SNRs using Eq. (17). This indicates that the high signal power supplied at the input is not reflected effectively at the receiver output. So, with less BS antennas (m), the asymptotic (high SNR) SER model in Eq. (18) is over-estimating the exact MM wave error performance represented by Eq. (17).

Conversely, Figure 16 depicts average and asymptotic (high SNR) SER comparisons in uplink scenarios for 2×20 equicorrelated MM wave MIMO under medium correlations $\sigma^2_{t/r} = \frac{\pi}{32}$ and assuming QPSK signals. With a higher number of BS antennas, i.e., $m = 20$, the MM wave system attains higher diversity levels. Therefore, greater MIMO gains will lead to higher probabilities of obtaining a weak faded path. Thus, in the asymptotic (high SNR) regime, received output power levels are more and thereby lower error levels are obtained using Eq. (17). Figure 16 shows lesser separations between exact and asymptotic (high SNR) SER. Therefore, with higher number of BS antennas (m), the asymptotic (high SNR) SER model in Eq. (18) properly estimates the actual error performance of equicorrelated MM wave system described by Eq. (17) in uplink scenarios.

4) DOWNLINK ASYMPTOTIC (HIGH SNR) SER ANALYSIS

In addition, asymptotic (high SNR) SER analysis is also carried out for MM wave MIMO-MRC link in case of downlink $m \times 2$ systems under similar conditions. Using

Eq. (18), MM wave SER (in asymptotic (high SNR) regime) is simulated and then observed with variations only in input SNR levels, $\overline{\gamma}$ for a fixed correlation level, specific modulation scheme and particular MIMO order. For practical demonstration of the asymptotic (high SNR) system behavior, finitely large input SNR values ranging upto as high as 20-30 dB are taken into account. Under such considerations, the asymptotic (high SNR) SERs obtained are compared with the average SERs evaluated from Eq. (17). Different representative cases by altering correlation levels, MIMO configurations, and modulation formats are observed to validate the study [15]. Table 3 accordingly showcases the downlink average and asymptotic SER levels for the proposed system through comparisons with uplink scenarios.

It is highly significant to note that beamsteering and equicorrelated MIMO modeling are incorporated in the proposed MM wave system by equally setting: (i) mean departure/arrival angles (in Section VI-B) from a pre-defined AoD/AoA dictionary (discussed in Section III-A) and (ii) transmit/receive variances (in Section VI-B). In addition to this, by maximally setting the transceiver variances (in Section VI-B), novel minimized equicorrelations are achieved from the MM wave setup. With significant reduction in transmit-receive correlation levels using this new method, a drastic performance improvement as compared to the existing MM wave systems is intuitively expected. Given this backdrop, it is vital to observe that the simulated SER curves nearly approximate straight lines or linear falls due to highly synchronized nature of transmission/reception using specific AoDs/AoAs. Such characteristics are observed with proper vector/angle tuning because the practical system precisely follows the theoretical model to achieve minimal transceiver equicorrelations. Further it is crucial to observe that some of the simulation results presented in this section do reflect SER levels as low as 10^{-40} (in order). Also, it is necessary to state here that even the previously proposed MM wave models which are non-minimally equicorrelated in nature showcase only fractionally higher SERs (in comparison to the current model) as can be observed in [65] and [66]. Therefore, the observation that the newly proposed MM wave system facilitating strong minimal correlation tuning exhibits steeply reduced SERs in practice with incredibly large orders of magnitude is quite as expected and also in line with the analytical study presented in Sections V and VI. Further, it is noteworthy that achieving drastically low SER levels down to 10^{-40} does involve the *tedious* task of simulating more than 10^{42} bits/symbols for 100 bit/symbol errors. However, such *intensive* computations are *necessary* for *proper visualisation* of significant error *reduction capabilities* exhibited by the proposed MM wave model. With *lesser* number of bits/symbols, such system abilities are *not prominent*. To ensure that processing *delays are minimum*, the large number of received bits/symbols are evaluated over *parallel batches* (under identical channel conditions) using *three* active cores of the Quad Core machine as discussed in Section VII-A. While demonstrating a drastic fall in SER,

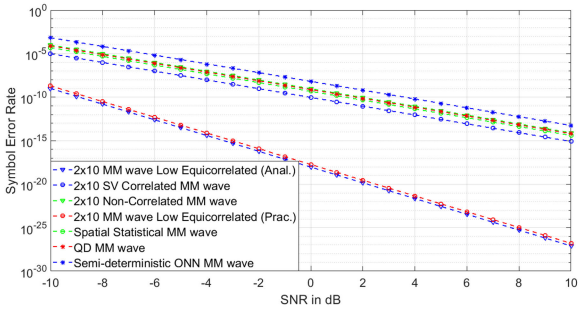

FIGURE 17. Average SER comparison for 2 × 10 QPSK MM wave MIMO with No correlation, Analytical Equicorrelation ($\rho_{min} = 0.2$), Practical Equicorrelation ($\sigma^2_{t/r_{min}} = \frac{\pi}{16}$), SV Correlation ($\sigma^{AoD}_{AS} = \sqrt{\frac{\pi}{32}}$, $\sigma^{AoA}_{AS} = \sqrt{\frac{\pi}{16}}$), Spatial Statistical MM wave, Semi-deterministic ONN MM wave and QD MM wave.

the MM wave system also showcases an acceptably low *MATLAB* (*tic-toc*) simulation time requirement of around 0.001285 *seconds*.

The illustrations in Sections VII-B1 to VII-B4 clearly signify that the receiver performance of MM wave MIMO links have direct dependency on antenna correlation levels. The MIMO-MRC reception quality metrics are observed to significantly improve with lower antenna correlations. Furthermore, at MM wave frequencies, with dependency of MIMO channel gains on antenna steering vectors and in turn system AoDs/AoAs [Eq. (2)], correlation measures could be effectively adjusted to lower prevailing inter-element correlations [Eqs. (4), (5)]. Following this, adequate SER performance improvements for MM wave models are achieved with accurately tuned AoDs/AoAs using Eqs. (17) and (18). Such control over output performance cannot be achieved in the non-MM wave regime with inter-antenna correlations being independent of tunable AoDs/AoAs. Thus, using this crucial dependance, a new minimal equicorrelation MIMO-MRC model is presented here to obtain reduced average SER levels during near-user beamsteered MM wave communications.

5) COMPARISON AND SIGNIFICANCE OF MINIMALLY EQUICORRELATED MODEL VERSUS EXISTING MODELS

Average SER levels for the proposed equicorrelation model described in Sections VI-A and VI-B are compared with those of existing SV correlation model for MM wave links discussed in [62] and [68]. Inter-element correlations are characterized for the later model in terms of mean departure angle ($\overline{\phi}_{AoD}$), mean arrival angle ($\overline{\phi}_{AoA}$), transmit angular deviation (σ^{AoD}_{AS}) and receive angular deviation (σ^{AoA}_{AS}) [62]. Higher deviations from the mean angle would result in spatially well-separated transmissions and thereby lower correlation levels. However, it is detrimental to note that, unlike the proposed minimal equicorrelation model, the SV model in [68] is non-equicorrelated in nature, indicating dissimilar correlations at the transmitter and receiver sides. Moreover, the analytical study in [62] for the later does not

TABLE 4. Average SER Comparison with Existing Methods.

S.No.	System Model	2×10 Uplink Average SER ($\overline{\gamma} = 2\ dB$, Modulation : BPSK)
1.	Learning based D2D MM wave [70]	3×10^{-4}
2.	Regularized LS MM wave [71]	7×10^{-5}
3.	Nakagami-m Multistate MM wave [72]	2×10^{-4}
4.	Generative Neural Network MM wave [73]	8×10^{-3}
5.	Spatial Statistical MM wave [74]	3×10^{-5}
6.	Semi-deterministic ONN MM wave [75]	9×10^{-4}
7.	QD MM wave [76]	6×10^{-5}
8.	Proposed Minimal Equicorrelation MM wave	5×10^{-9}

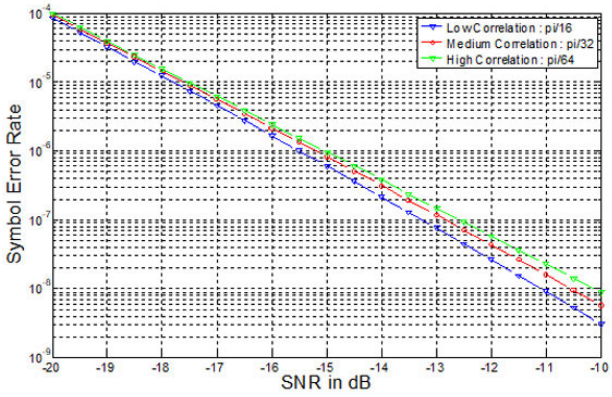

FIGURE 18. SER variation with correlation for 2 × 3 Equicorrelated MM wave BPSK MIMO in low SNR region.

focus on any method to equally minimize correlations at both ends as highlighted for the proposed model in Section VI-B. Therefore, effective tuning of system vectors (or transmission angles) to achieve reduced correlations and thereby reduced SER measures is not possible using the SV model [69].

Figure 17 compares average SER levels for a 2×10 QPSK MM wave MIMO system without considering correlations, with SV correlations reflected by $\sigma_{AS}^{AoD} = \sqrt{\frac{\pi}{32}}$ and $\sigma_{AS}^{AoA} = \sqrt{\frac{\pi}{16}}$, with minimal analytic ($\rho = 0.2$) and practical ($\sigma_{t/r}^2 = \frac{\pi}{16}$) equicorrelations. It also depicts SER comparisons between the Minimal Correlation system and recently proposed Spatial Statistical, Semi-deterministic ONN and QD MM wave models [74], [75], [76]. Whereas the inferences drawn from these comparisons have been elaborated in the next paragraph, the discussion here throws light at SER performance levels for the proposed system, SV correlated model and Non-Correlated model. For SV model, the mean transmit AoD i.e. $\overline{\phi}_{AoD}$ and receive AoA i.e. $\overline{\phi}_{AoA}$ are both assumed to be $\frac{\pi}{2}$. However, due to non-equicorrelated nature, the transmit deviation (σ_{AS}^{AoD}) is lesser signifying higher correlations and receive deviation is greater representing lower correlations. In the proposed equicorrelation model, mean AoD/AoA i.e. $\theta_{t/r}$ are both assumed to be $\frac{\pi}{2}$. Due to lower correlations prevalent at receive side, the MM wave SV correlated system exhibits marginally reduced SER levels as compared to the non-correlated MM wave system. This is in agreement with the discussion in [62]. However, no further performance tuning is possible [68]. On the other hand, it is crucial to observe that the proposed equicorrelated system with minimal correlations at both transmit and receive ends achieves a significant decrease in MM wave SER levels as compared to the non-correlated and SV-correlated systems [5] [62]. The depicted performance gains using proposed model are obtained as a result of transmission and reception at properly tuned departure and arrival angles, ($\theta_{t_{mod}}$ and $\theta_{r_{mod}}$) computed using Eqs. (24) and (25) in Section VI-B. Additionally, it may be noted from Figure 17 that under low equicorrelations, the simulated curves for MM wave average SER levels are in agreement with the analytical curves. This validates performance gains proposed using Minimal Equicorrelation model for short range NLOS MM wave users. Also, the practical SER levels exhibited are fractionally higher than the analytical measures as expected.

Quite similar to Figure 17, average SER levels for the Minimal Equicorrelation system are compared with those of other recently proposed MM wave channel models [70], [71], [72], [73], [74], [75], [76] in Table 4. The analysis is carried out considering uplink scenario with $m = 10$. The input SNR, $\overline{\gamma}$ is set to 2 dB and BPSK modulated signals are considered. From both Table 4 and Figure 17, it can be clearly observed that the non-equicorrelated MM wave models presented in [62], [70], [71], [72], [73], [74], [75], and [76] exhibit higher average SER levels without any method presented to tune the performance of such systems. On the other hand, significantly reduced average SER levels are achieved using the proposed Minimal Equicorrelation model through transmission and reception at tuned departure/arrival angles.

It is highly significant to note in Figure 18 that the proposed system depicts reduced average SER even under scarce SNR in the range of $-20\ dB$ to $-10\ dB$ with minimal correlation tuning. At significantly low SNR of $-10\ dB$ also, the presented MM wave model can be effectively utilized to achieve SER improvements (through reduced correlations via angular tuning) which would also be highly beneficial for remote wireless applications such as satellite and underwater communications [45]. Such performance improvements achieved at scarce SNR levels through newly introduced minimized equicorrelations strongly establishes the proposed system's novel contribution over existing methods cited in [70], [71], [72], [73], [74], [75], and [76].

VIII. CONCLUSION

The work put forward emphasizes devising means to enhance SER performance in millimeter wave receivers. In line with this, channel modelling is performed, taking into account short-range NLOS users. Vital stochastic models presented for MM wave links are analyzed and reveal the vital

dependance of such taps on transmit-receive steering vectors or AoDs/AoAs. Furthermore, this throws light on controlled MM wave correlation measures obtained using effectively steered AoDs and AoAs. This is applicable only to MM wave communications and does not hold in the case of microwave transmissions. Depending on the same, novel minimal equicorrelations in MM wave MIMO-MRC systems are proposed in this paper, showcasing SER reductions for near users in beamsteering based NLOS links. Reduced equicorrelations are suggested to be practically realized through effective tuning of AoDs and AoAs, utilizing adjustable antenna systems for 5G and beyond. The performance of the proposed model could be further analyzed for distant users by applying appropriate beamforming methods.

APPENDIX

Various mathematical derivations and computations related to this paper have been presented here.

A. DEDUCTION OF BEAMSPACE MM WAVE MIMO CHANNEL MATRIX

Utilizing Eq. (1), the solid angles are obtained as depicted in Eq. (28)

$$\theta_i = \arcsin(\frac{\lambda v_i}{d}) \tag{28}$$

with, $\lambda = \frac{c}{f_{MM}}$ as the operating wavelength, d being the spacing between two elements in a Uniform Linear Array (ULA) comprising of N elements, c signifying the speed of light and f_{MM} representing the MM wave carrier frequency. For such geometries, the vector used to steer the phased array towards θ_i direction is calculated by using Eq. (29).

$$a(\theta_i) = [1, e^{-j2\pi v_i}, e^{-j4\pi v_i}, \cdots e^{-j2\pi v_i(N-1)}]^T \tag{29}$$

The angular spacings are virtually uniform and result in steering vectors that correspond to θ_i forming an orthonormal basis function U. This $N \times N$ matrix, U can be mathematically expressed as shown in Eq. (30).

$$U = \frac{1}{\sqrt{N}}\Big[\{a(\theta_0)\}\{a(\theta_1)\}\cdots\{a(\theta_{N-1})\}\Big]^T \tag{30}$$

where, $\{a(\theta_0)\}$ is the $N \times 1$ steering vector corresponding to first antenna element, $\{a(\theta_1)\}$ represents the same for second element and so on upto the N^{th} element with each being a column in the matrix U. $[\cdot]^T$ denotes matrix transpose operation. At both transmit and receive sides, the orthonormal matrix U is characterized by U_T and U_R respectively. U has a DFT (unitary) nature with diagonal elements set to unity [5], [8], [15]. Thus, it fulfils the condition mentioned in Eq. (31).

$$U^*U = UU^* = I \tag{31}$$

Considering the narrowband representation of MIMO, the MM wave channel in beamspace mode is expressed using Eq. (32) where H_b signifies different MIMO tap gains [5], [6].

$$H_{MM} = U_R H_b U_T^* \tag{32}$$

Moreover, the channel model in MM wave regime can be modeled as a function of transceiver steering vectors as illustrated in Eq. (33)

$$H_{MM} = \sum_{i=1}^{N_r}\sum_{k=1}^{N_t}[H_b]_{i,k}a_R(\theta_{R,i})a_T(\theta_{T,k}) \tag{33}$$

where, $\theta_{R,i}$ and $\theta_{T,k}$ are the arrival and departure angles respectively. $a_R(\theta_{R,i})$ and $a_T(\theta_{T,k})$ are the vectors used to steer the wave at receive and transmit side. In the presented work, $a_R(\theta_{R,i})$ and $a_T(\theta_{T,k})$ are utilized to steer the signals purposely in the direction of desired user i.e. θ_d [12].

MM wave transmissions being characterized by limited multipaths [5], the narrowband channel at such frequencies can be expressed in terms of N_p paths using Eq. (34).

$$H_{MM} = \sum_{k=1}^{N_p}\alpha_k a_R\left(\theta_{R,k}\right)a_T^*\left(\theta_{T,k}\right) \tag{34}$$

with α_k being the tap gain, $\theta_{R,k}$ denoting the receiver arrival angle and $\theta_{T,k}$ signifying the transmit departure angle for k^{th} multipath. $a_T(\theta_{T,k})$ is the transmit steering vector of dimension $N_T \times 1$ and $a_R(\theta_{R,k})$ is the $N_R \times 1$ receive response vector respectively [18], [19], [20], [21], [22].

With the assumption of 2×2 MIMO and using Eq. (32), the MIMO channel gains can be represented by Eq. (35)

$$H_b = \begin{bmatrix} h_{11} & h_{12} \\ h_{21} & h_{22} \end{bmatrix} \tag{35}$$

The illustrations in [5] reveal that the orthonormal basis function [23], [24], [25], [26], U can be further expressed using Eq. (36)

$$U = \frac{1}{\sqrt{N}}[\{a(\theta_0)\}\{a(\theta_1)\}]^T \tag{36}$$

where $a(\theta_0)$ and $a(\theta_1)$ denote steering vectors for first and second elements of the array. U can be replicated at transmit and receive sides utilizing Eqs. (37) and (38).

$$U_T = \frac{1}{\sqrt{N_T}}[\{a_T(\theta_0)\}\{a_T(\theta_1)\}]^T \tag{37}$$

$$U_R = \frac{1}{\sqrt{N_R}}[\{a_R(\theta_0)\}\{a_R(\theta_1)\}]^T \tag{38}$$

In case of U_T and also U_R, $\{a_T(\theta_i)\}$ and $\{a_R(\theta_i)\}$ are $N_T \times 1$ and $N_R \times 1$ vectors each owing to N_T and N_R transmit-receive elements respectively [2], [7], [27], [28], [29], [30]. Therefore, elaborating Eq. (37) further, Eqs. (39) and (40) are deduced.

$$U_T = \frac{1}{\sqrt{N_T}}\begin{bmatrix} a_{T_1}(\theta_0) & a_{T_1}(\theta_1) \\ a_{T_2}(\theta_0) & a_{T_2}(\theta_1) \end{bmatrix}^T \tag{39}$$

$$\Rightarrow U_T = \frac{1}{\sqrt{N_T}}\begin{bmatrix} a_{T_1}(\theta_0) & a_{T_2}(\theta_0) \\ a_{T_1}(\theta_1) & a_{T_2}(\theta_1) \end{bmatrix} \tag{40}$$

Similar expansion of Eq. (38) yields Eq. (41).

$$U_R = \frac{1}{\sqrt{N_R}}\begin{bmatrix} a_{R_1}(\theta_0) & a_{R_2}(\theta_0) \\ a_{R_1}(\theta_1) & a_{R_2}(\theta_1) \end{bmatrix} \tag{41}$$

U_T and U_R are therefore $N_T \times N_T$ and $N_R \times N_R$ matrices respectively [5]. Furthermore, using Eqs. (40) and (41) in Eq. (32), we can evaluate the MM wave MIMO matrix H_{MM} as follows.

$$\begin{aligned} H_{MM} &= \frac{1}{\sqrt{N_R N_T}} \begin{bmatrix} a_{R_1}(\theta_0) & a_{R_2}(\theta_0) \\ a_{R_1}(\theta_1) & a_{R_2}(\theta_1) \end{bmatrix} \begin{bmatrix} h_{11} & h_{12} \\ h_{21} & h_{22} \end{bmatrix} \\ &\quad \cdot \begin{bmatrix} a_{T_1}(\theta_0) & a_{T_2}(\theta_0) \\ a_{T_1}(\theta_1) & a_{T_2}(\theta_1) \end{bmatrix}^* \\ \Rightarrow H_{MM} &= \frac{1}{\sqrt{N_R N_T}} \begin{bmatrix} a_{R_1}(\theta_0) & a_{R_2}(\theta_0) \\ a_{R_1}(\theta_1) & a_{R_2}(\theta_1) \end{bmatrix} \begin{bmatrix} h_{11} & h_{12} \\ h_{21} & h_{22} \end{bmatrix} \\ &\quad \cdot \begin{bmatrix} a^*_{T_1}(\theta_0) & a^*_{T_1}(\theta_1) \\ a^*_{T_2}(\theta_0) & a^*_{T_2}(\theta_1) \end{bmatrix} \\ \Rightarrow H_{MM} &= \frac{1}{\sqrt{N_R N_T}} \begin{bmatrix} A & B \\ C & D \end{bmatrix} \end{aligned} \tag{42}$$

where,

$$\begin{aligned} A &= a^*_{T_1}(\theta_0)a_{R_1}(\theta_0)h_{11} + a^*_{T_1}(\theta_0)a_{R_2}(\theta_0)h_{21} \\ &\quad + a^*_{T_2}(\theta_0)a_{R_1}(\theta_0)h_{12} + a^*_{T_2}(\theta_0)a_{R_2}(\theta_0)h_{22} \\ B &= a^*_{T_1}(\theta_1)a_{R_1}(\theta_0)h_{11} + a^*_{T_1}(\theta_1)a_{R_2}(\theta_0)h_{21} \\ &\quad + a^*_{T_2}(\theta_1)a_{R_1}(\theta_0)h_{12} + a^*_{T_2}(\theta_1)a_{R_2}(\theta_0)h_{22} \\ C &= a^*_{T_1}(\theta_0)a_{R_1}(\theta_1)h_{11} + a^*_{T_1}(\theta_0)a_{R_2}(\theta_1)h_{21} \\ &\quad + a^*_{T_2}(\theta_0)a_{R_1}(\theta_1)h_{12} + a^*_{T_2}(\theta_0)a_{R_2}(\theta_1)h_{22} \\ D &= a^*_{T_1}(\theta_1)a_{R_1}(\theta_1)h_{11} + a^*_{T_1}(\theta_1)a_{R_2}(\theta_1)h_{21} \\ &\quad + a^*_{T_2}(\theta_1)a_{R_1}(\theta_1)h_{12} + a^*_{T_2}(\theta_1)a_{R_2}(\theta_1)h_{22} \end{aligned}$$

Eq. (42) represents the finalized Beamspace MM wave 2×2 MIMO channel matrix which can be easily extended for an arbitrary $N_T \times N_R$ system.

B. FADING CORRELATION STATISTICS

It is of prime importance to characterize the proposed MM wave link as an L tap multipath channel for analyzing the background fading-correlation statistics [5], [10]. In general, the l^{th} tap for a MM wave channel, H_{MM} is expressed as the sum of a fixed (possibly LOS) component $\bar{H_{MM_l}} = E[H_{MM_l}]$ ($E[\cdot]$ is the expectation operator) and a variable (scattered, NLOS) component $\tilde{H_{MM_l}}$ depicted below with $l = 0, 1, \cdots, L-1$.

$$H_{MM_l} = \bar{H_{MM_l}} + \tilde{H_{MM_l}} \tag{43}$$

For the proposed NLOS MM wave, we have Rayleigh faded MIMO taps (H_R) with $\bar{H_{MM_l}} = O_{N_R \times N_T}$ and therefore $H_{MM_l} = \tilde{H_{MM_l}}$. Here, $O_{N_R \times N_T}$ is the Zero matrix of size $N_R \times N_T$. Further, elements of the matrix, $\tilde{H_{MM_l}}$ (which are possibly correlated) are considered to be circularly symmetric Gaussian random variables. However, each path l is assumed uncorrelated from the path k so that the following holds for all $l \neq k$.

$$E\{vec(\tilde{H_{MM_l}})(vec(\tilde{H_{MM_k}}))^H\} = O_{N_R N_T \times N_R N_T} \tag{44}$$

where, $vec(\cdot)$ represents column wise vector-stacking of a matrix and $(\cdot)^H$ denotes the matrix Hermitian operation. Also, each path l is represented by: (i) mean departure angle, $\bar{\theta_{T,l}}$, (ii) mean arrival angle, $\bar{\theta_{R,l}}$, (iii) transmit angular variance, $\sigma^2_{\theta_{T,l}}$, (iv) receive angular variance, $\sigma^2_{\theta_{R,l}}$ and (v) path gain, σ^2_l (evaluated based on channel power delay profile). Now, considering double correlated environments, the Rayleigh component of l^{th} tap is decomposed as below for $l = 0, 1, \cdots, L-1$.

$$\tilde{H_{MM_l}} = R_l^{\frac{1}{2}} \tilde{H_{MM_{w,l}}} (S_l^{\frac{1}{2}})^T \tag{45}$$

Here, $R_l = R_l^{\frac{1}{2}} R_l^{\frac{1}{2}}$ and $S_l = S_l^{\frac{1}{2}} S_l^{\frac{1}{2}}$ are the receive and transmit correlation matrices corresponding to $\tilde{H_{MM_l}}$, $\tilde{H_{MM_{w,l}}}$ is an $N_R \times N_T$ matrix with i.i.d. $\mathcal{CN}(0, \sigma_l^2)$ entries, $(\cdot)^{\frac{1}{2}}$ denotes the Hermitian square root of a matrix, $(\cdot)^T$ signifies matrix transpose and $\mathcal{CN}(\cdot, \cdot)$ represents Complex Normally distributed random variables of specified mean and variance. It is a key to note here that the power delay profile, σ_l^2 has been incorporated in the entries of $\tilde{H_{MM_{w,l}}}$. From the above discussion, it is also known that $E\{vec(\tilde{H_{MM_l}})(vec(\tilde{H_{MM_k}}))^H\} = O_{N_R N_T \times N_R N_T}$ for all $l \neq k$. As per the elaborations laid down in [67], the fading correlation between two antenna elements spaced $s\Delta$ wavelengths apart is defined as $\rho(s\Delta, \bar{\theta}, \sigma_\theta)$. Respectively, for the transmit and receive antenna elements, we have, for $0 \leq l \leq L-1$, $\rho(s\Delta_T, \bar{\theta_{T,l}}, \sigma_{\theta_{T,l}}) = E\{[\tilde{H}_l]_{k_1,r}[\tilde{H}_l]^*_{k_1,r+s}\}$ ($0 \leq k_1 \leq N_R - 1$, $0 \leq r \leq N_T - s - 1$) and $\rho(s\Delta_R, \bar{\theta_{R,l}}, \sigma_{\theta_{R,l}}) = E\{[\tilde{H}_l]_{r,k_1}[\tilde{H}_l]^*_{r+s,k_1}\}$ ($0 \leq k_1 \leq N_T - 1$, $0 \leq r \leq N_R - s - 1$). $(\cdot)^*$ denotes matrix conjugate operation. Following the deductions in [67], the correlation matrices R_l and S_l are subsequently expressed as below.

$$[R_l]_{m_1,n_1} = \rho((n_1 - m_1)\Delta_R, \bar{\theta_{R,l}}, \sigma_{\theta_{R,l}}) \tag{46}$$

$$[S_l]_{m_1,n_1} = \rho((n_1 - m_1)\Delta_T, \bar{\theta_{T,l}}, \sigma_{\theta_{T,l}}) \tag{47}$$

Further, we consider that the effective angles of departure and arrival corresponding to the l^{th} path are given by $\theta_{T,l} = \bar{\theta_{T,l}} + \hat{\theta_{T,l}}$ and $\theta_{R,l} = \bar{\theta_{R,l}} + \hat{\theta_{R,l}}$ with $\hat{\theta_{T,l}} \sim \mathcal{N}(0, \sigma^2_{\theta_{T,l}})$ and $\hat{\theta_{R,l}} \sim \mathcal{N}(0, \sigma^2_{\theta_{R,l}})$. Given this background, it has already been demonstrated in [67] that $\rho(s\Delta, \bar{\theta}, \sigma_\theta)$ may be expressed as below.

$$\rho(s\Delta, \bar{\theta}, \sigma_\theta) \approx e^{-j2\pi s\Delta \cos(\bar{\theta})} e^{-\frac{1}{2}(2\pi s\Delta \sin(\bar{\theta})\sigma_\theta)^2} \tag{48}$$

The results stated above shall be used for straightforward deduction of practical transceiver correlation matrices applicable to the proposed minimally equicorrelated MM wave model [5], [11].

C. CUMMULATIVE MAXIMUM EIGEN DISTRIBUTIONS FOR KRONECKER CORRELATED COMPLEX WISHART MATRICES

Generalized results for maximum eigen mode statistical distributions of complex Wishart matrices under separate correlation environments are presented here. The closed form expressions analyzed here are used to examine correlated MIMO-MRC performance under NLOS MM wave transmission scenarios.

We consider $X \sim \mathcal{CN}_{m,n}(O_{m\times n}, \Sigma \bigotimes \Omega)$ for $n \leq m$ with $\Omega \in C^{n\times n}$ and $\Sigma \in C^{m\times m}$ being positive Hermitian definite matrices defined by respective eigen values $\omega_1 < \cdots < \omega_n$ and $\sigma_1 < \cdots < \sigma_m$. Thus, the highest eigen value λ_m evaluated from Wishart matrix $X^\dagger X$ has a CDF analytically represented by Eq. (49). The same is vital in examining MM wave system performance [10], [43].

$$F_{\lambda_m}(x) = \frac{(-1)^n \Gamma_n(n) det(\Omega)^{n-1} det(\Sigma)^{m-1} det(\Psi(x))}{\Delta_n(\Omega)\Delta_m(\Sigma)(-x)^{\frac{n(n-1)}{2}}} \tag{49}$$

Here, $\Gamma_n(\cdot)$ is a complex Gamma multivariate function mathematically expressed by Eq. (50).

$$\Gamma_n(n) = \prod_{i=1}^{n} \Gamma(n-i+1) \tag{50}$$

Moreover, $\Delta_m(\cdot)$ is termed as Vandermonde determinant calculated on eigenvalues of m-dimensional argument for Σ matrix. Numerically, it is evaluated using Eq. (51).

$$\Delta_m(\Sigma) = \prod_{i<j}^{m} (\sigma_j - \sigma_i) \tag{51}$$

Also, the $\Psi(x)$ matrix of dimension $m \times m$ is expressed in terms of its $(i,j)^{th}$ element by Eq. (52).

$$(\Psi(x))_{i,j} = \begin{cases} (\frac{1}{\sigma_j})^{m-i}, & i \leq \tau \\ e^{\frac{-x}{\omega_{i-\tau}\sigma_j}} \wp(m; \frac{-x}{\omega_{i-\tau}\sigma_j}), & i > \tau \end{cases} \tag{52}$$

where, $\tau = m - n$. Further, $\wp(\cdot;\cdot)$ in Eq. (53) denotes the incomplete gamma function with lower regularization.

$$\wp(l; y) = 1 - e^{-y} \sum_{k=0}^{l-1} \frac{y^k}{k!} \tag{53}$$

Considering a case where $n = 2$ and $m \geq 2$, Eq. (49) can be simplified and re-written as Eq. (54).

$$F_{\lambda_m}(x) = \frac{det(\Omega)}{\Delta_2(\Omega)\Delta_m(\Sigma)} \sum_{p=1}^{m} \sum_{t=1, t\neq p}^{m} (-1)^{p+\phi(t)} (\sigma_p \sigma_t)^{m-1} \times \Delta_{m-2}(\sigma^{[p,t]}) \cdot Q_{p,t}(x) \tag{54}$$

where, $\phi(t)$ is calculated using Eq. (55)

$$\phi(t) = \begin{cases} t, & t < p \\ t-1, & t > p \end{cases} \tag{55}$$

Also, $\sigma^{[p,t]} = \{\sigma_i; i \in \{1, \cdots, m\} \backslash \{p, t\}\}$ and $Q_{p,t}(x)$ is represented by Eq. (56)

$$Q_{p,t}(x) = \frac{1}{x} e^{-\frac{x}{\omega_2 \sigma_p}} \wp(m; -\frac{x}{\omega_2 \sigma_p}) e^{-\frac{x}{\omega_1 \sigma_t}} \wp(m; -\frac{x}{\omega_1 \sigma_t}) \tag{56}$$

Furthermore, with $n = m = 2$, Eq. (49) will get reduced to a simpler form as shown in Eq. (57). Both the simplified closed forms presented for $F_{\lambda_m}(x)$ in Eqs. (54) and (57) are used to derive crucial MM wave receiver metrics [10], [12].

$$F_{\lambda_m}(x) = \frac{\omega_1\omega_2\sigma_1\sigma_2}{x(\sigma_2-\sigma_1)(\omega_2-\omega_1)} \sum_{i=1}^{2} (-1)^i \prod_{j=1}^{2} (e^{-\frac{x}{\omega_{|i-j|+1}\sigma_j}} + \frac{x}{\omega_{|i-j|+1}\sigma_j} - 1) \tag{57}$$

D. AVERAGE SER DEDUCTION OF PROPOSED MM WAVE SYSTEM

Let us consider all general modulation formats that have an SER expression as shown in Eq. (58).

$$P_S = E_\gamma \left[aQ(\sqrt{2b\gamma}) \right] \tag{58}$$

where, $Q(\cdot)$ denotes the Gaussian Q-function and a, b are constants that indicate the modulation method used [15]. Exact SER expressions are presented for BPSK (a=1, b=1), orthogonal signaling (OS) BFSK (a=1, b=0.5), minimum correlation (MC) BFSK (a=1, b=0.715) and M-ary PAM ($a = \frac{2(M-1)}{M}$, $b = \frac{3}{M^2-1}$) schemes [10], [15]. Moreover, in case of modulation formats for which Eq. (58) is an approximation i.e. M-ary PSK ($a = 2$, $b = \sin^2(\frac{\pi}{M})$), the proposed closed forms will yield approximate SER levels [43]. To deduce the average SER for MIMO-MRC under MM wave regime, results of baseline work referred in [10] for semi-correlated channels are generalized under double correlated environments [15], [43].

Firstly, the Gaussian Q-function in Eq. (58) can be generally expressed in terms of any arbitrary parameter x by utilizing a dummy variable v for mathematical consistency as shown below in Eq. (59).

$$Q(x) = \frac{1}{\sqrt{\pi}} \int_{\frac{x}{\sqrt{2}}}^{\infty} e^{\frac{-v^2}{2}} dv \tag{59}$$

Specific to the problem at hand, $Q(\cdot)$ in Eq. (59) can be re-expressed in terms of γ by putting $x = \sqrt{2b\gamma}$. Further, by replacing the value of $Q(x)$ from Eq. (59), we can re-write Eq. (58) as Eq. (60). To facilitate evaluation of the outer integral in Eq. (60), another dummy variable u is used in place of γ. Also, $f_\gamma(\gamma)$ in Eq. (60) denotes the PDF of output SNR, γ.

$$P_S = \frac{a}{\sqrt{\pi}} \int_0^\infty \left[\int_{\sqrt{bu}}^{\infty} e^{-v^2} dv \right] f_\gamma(u) du \tag{60}$$

To solve the RHS of Eq. (60) using integration by parts, we initially differentiate the term within square brackets as

below.

$$\begin{aligned}\frac{d}{du}\left[\int_{\sqrt{bu}}^{\infty} e^{-v^2}dv\right] &= -\frac{d}{du}\left[\int_{0}^{\sqrt{bu}} e^{-v^2}dv\right] \\ &= -\frac{d}{du}\sqrt{bu}\left(\frac{d}{dx}\left[\int_{0}^{x} e^{-v^2}dv\right]\right)_{x=\sqrt{bu}} \\ &= -\frac{1}{2}\sqrt{\frac{b}{u}}e^{-bu} \end{aligned} \tag{61}$$

In Eq. (61), the first step is obtained from the result presented in Eq. (62) whereas the second and third steps are derived using Chain rule and Second Fundamental Theorem of calculus respectively [3], [12].

$$\int_{0}^{\infty} e^{-v^2}dv = \frac{\sqrt{\pi}}{2} \tag{62}$$

Using Eqs. (60) and (61), we obtain Eq. (63) as below.

$$P_S = \frac{a\sqrt{b}}{2\sqrt{\pi}}\int_{0}^{\infty}\frac{e^{-bu}}{\sqrt{u}}F_{\gamma}(u)du \tag{63}$$

Eq. (63) generalizes semi-correlated average SER expressions of the baseline model referred in [10] under MM wave separately correlated Rayleigh environments [5], [11]. Further, we utilize the CDF of λ_m in Eq. (54) to re-write Eq. (63) as Eq. (64)

$$P_S = \frac{a\sqrt{b}}{2\sqrt{\pi}}\int_{0}^{\infty}\frac{e^{-bu}}{\sqrt{u}}F_{\lambda_m}(\frac{u}{\overline{\gamma}})du \tag{64}$$

Next, a modified expression is deduced for $Q_{p,t}(x)$ illustrated in Eq. (56). By expansion of the exponentials into power series and utilizing Eq. (53), Eq. (56) is expressed as Eq. (65)

$$\begin{aligned} Q_{p,t}(x) &= \frac{1}{x}\left(\sum_{k=m}^{\infty}\frac{\left(\frac{-x}{\omega_2\sigma_p}\right)^k}{k!}\right)\left(\sum_{k=m}^{\infty}\frac{\left(\frac{-x}{\omega_1\sigma_t}\right)^k}{k!}\right) \\ &= \frac{1}{x}\sum_{k_1=m}^{\infty}\sum_{k_2=m}^{\infty}\frac{(-x)^{k_1+k_2}\left(\frac{1}{\omega_2\sigma_p}\right)^{k_1}\left(\frac{1}{\omega_1\sigma_t}\right)^{k_2}}{k_1!k_2!} \\ &= -\sum_{k=2m}^{\infty}(-x)^{k-1}S_k \end{aligned} \tag{65}$$

where,

$$S_k = \sum_{l=m}^{k-m}\frac{\left(\frac{1}{\omega_2\sigma_p}\right)^l\left(\frac{1}{\omega_1\sigma_t}\right)^{k-l}}{l!(k-l)!} \tag{66}$$

Further, replacing Eq. (65) in Eqs. (54) and (63), the average SER can be expressed as shown in Eq. (67)

$$P_S = \frac{a\sqrt{b}}{2\sqrt{\pi}}\frac{det(\Omega)}{\Delta_2(\Omega)\Delta_m(\Sigma)}\sum_{p=1}^{m}\sum_{t=1,t\neq p}^{m}(-1)^{p+\phi(t)}(\sigma_p\sigma_t)^{m-1} \cdot \Delta_{m-2}(\sigma^{[p,t]})T \tag{67}$$

Here, T is represented using Eq. (68) as below.

$$\begin{aligned} T &= \int_{0}^{\infty}\frac{e^{-bu}}{\sqrt{u}}Q_{p,t}(\frac{u}{\overline{\gamma}})du \\ &= -\sum_{k=2m}^{\infty}S_k\left(-\frac{1}{\overline{\gamma}}\right)^{k-1}\int_{0}^{\infty}u^{k-\frac{3}{2}}e^{-bu}du \\ &= \overline{\gamma}\sqrt{b}\sum_{k=2m}^{\infty}S_k\left(-\frac{1}{b\overline{\gamma}}\right)^k\Gamma\left(k-\frac{1}{2}\right) \end{aligned} \tag{68}$$

The last line of Eq. (68) is derived based on the well-known integration identity presented in Eq. (3.381.4) of the cited work [21] in our baseline paper [10]. We express S_k of Eq. (66) using Binomial expansion to eliminate the infinite summation as below in Eq. (69)

$$\begin{aligned} S_k = \frac{1}{k!}\Bigg(&\left(\frac{1}{\omega_2\sigma_p}+\frac{1}{\omega_1\sigma_t}\right)^k \\ &-\sum_{l=0}^{m-1}\binom{k}{l}\left(\frac{1}{\omega_2\sigma_p}\right)^l\left(\frac{1}{\omega_1\sigma_t}\right)^{k-l} \\ &-\sum_{l=k-m+1}^{k}\binom{k}{l}\left(\frac{1}{\omega_2\sigma_p}\right)^l\left(\frac{1}{\omega_1\sigma_t}\right)^{k-l}\Bigg) \end{aligned} \tag{69}$$

On replacing the variable l by $k-l$ in the second summation of Eq. (69), and following the property $\binom{k}{l} = \binom{k}{k-l}$, we can re-write S_k as in Eq. (70)

$$\begin{aligned} S_k = \frac{1}{k!}\Bigg(&\left(\frac{1}{\omega_2\sigma_p}+\frac{1}{\omega_1\sigma_t}\right)^k - \sum_{l=0}^{m-1}\binom{k}{l}\Bigg(\left(\frac{1}{\omega_2\sigma_p}\right)^l \\ &\cdot\left(\frac{1}{\omega_1\sigma_t}\right)^{k-l} + \left(\frac{1}{\omega_1\sigma_t}\right)^l\left(\frac{1}{\omega_2\sigma_p}\right)^{k-l}\Bigg)\Bigg) \end{aligned} \tag{70}$$

The representation of S_k in Eq. (70) is more convenient than the one in Eq. (66) because the limits of summation are independent of the term k. Further, Eq. (70) is substituted into Eq. (68) and thus we obtain Eq. (71)

$$\begin{aligned} T = \overline{\gamma}\sqrt{b}\Bigg(&\eta\left(0, -\frac{1}{\overline{\gamma}b}\left(\frac{1}{\omega_2\sigma_p}+\frac{1}{\omega_1\sigma_t}\right)\right) \\ &-\sum_{l=0}^{m-1}\frac{1}{l!}\frac{\eta\left(l, -\frac{1}{\overline{\gamma}b\omega_2\sigma_p}\right)}{(\overline{\gamma}b\omega_1\sigma_t)^l} - \sum_{l=0}^{m-1}\frac{1}{l!}\frac{\eta\left(l, -\frac{1}{\overline{\gamma}b\omega_1\sigma_t}\right)}{(\overline{\gamma}b\omega_2\sigma_p)^l}\Bigg) \end{aligned} \tag{71}$$

where,

$$\begin{aligned} \eta(l,y) &= \sum_{k=2m}^{\infty}\frac{y^{k-l}\Gamma\left(k-\frac{1}{2}\right)}{(k-l)!} \\ &= \sum_{k=2m-l}^{\infty}\frac{y^k\Gamma\left(k+l-\frac{1}{2}\right)}{k!} \\ &= \Gamma(l-\frac{1}{2})_1F_0(l-\frac{1}{2};y) \\ &\quad -\sum_{k=0}^{2m-l-1}\frac{y^k\Gamma(k+l-\frac{1}{2})}{k!} \end{aligned} \tag{72}$$

Here, ${}_1F_0(\cdot)$ denotes the hypergeometric binomial function. Also, keeping in mind that ${}_1F_0(a;y) = {}_2F_1(a;b;b;y)$ and utilizing Eq. (15.1.8) of cited work [22] in our baseline model [10], we further derive Eq. (73)

$$\eta(l,y) = \Gamma\left(l-\frac{1}{2}\right)(1-y)^{\frac{1}{2}-l} - \sum_{k=0}^{2m-l-1}\frac{y^k\Gamma(k+l-\frac{1}{2})}{k!} \tag{73}$$

Next, we utilize the identity as depicted in Eq. (74)

$$\Gamma(k+\frac{1}{2}) = \frac{(2k-1)!!\sqrt{\pi}}{2^k} \tag{74}$$

with,

$$(2k-1)!! \cong 1\times 3\times\cdots\times(2k-1) \tag{75}$$

Considering $k > 0$ and setting $(-1)!! = 1$ and $(-3)!! = -1$ yields Eq. (76)

$$\eta(l,y) = \frac{\sqrt{\pi}}{2^{l-1}}\tilde{\eta}(l,y) \tag{76}$$

where, $\tilde{\eta}(l,y)$ is represented by Eq. (77)

$$\tilde{\eta}(l,y) = (2l-3)!!(1-y)^{\frac{1}{2}-l} - \sum_{k=0}^{2m-l-1}\left(\frac{y}{2}\right)^k \cdot\frac{(2(k+l)-3)!!}{k!} \tag{77}$$

Eventually, putting the value of Eq. (77) into Eq. (71) and further solving Eq. (67), we obtain the finalized closed form expression for average SER of MM wave MIMO-MRC system under separately correlated NLOS (Rayleigh) MM wave channels as expressed in Eq. (78)

$$\begin{aligned}\left(P_{S,MM}\right)_{av} &= \frac{det(\Omega)ab\overline{\gamma}}{\Delta_2(\Omega)\Delta_m(\sum)}\sum_{p=1}^{m}\sum_{t=1,t\neq p}^{m}(-1)^{p+\phi(t)}(\sigma_p\sigma_t)^m \\ &\cdot(\sigma_p\sigma_t)^{-1}\Delta_{m-2}(\sigma^{[p,t]}) \\ &\times\left(\tilde{\eta}\left(0,-\frac{1}{\overline{\gamma}b}\left(\frac{1}{\omega_2\sigma_p}+\frac{1}{\omega_1\sigma_t}\right)\right)\right. \\ &\left.-\sum_{l=0}^{m-1}\frac{1}{l!}\frac{\tilde{\eta}\left(l,-\frac{1}{\overline{\gamma}b\omega_2\sigma_p}\right)}{(2\overline{\gamma}b\omega_1\sigma_t)^l}-\sum_{l=0}^{m-1}\frac{1}{l!}\frac{\tilde{\eta}\left(l,-\frac{1}{\overline{\gamma}b\omega_1\sigma_t}\right)}{(2\overline{\gamma}b\omega_2\sigma_p)^l}\right)\end{aligned} \tag{78}$$

E. ASYMPTOTIC (HIGH SNR) SER DERIVATION OF CORRELATED MM WAVE MODEL

On proper inspection of the MM wave average SER expression depicted using Eqs. (67) and (68), it can be observed that irrespective of the input SNR value $\overline{\gamma}$, the net contribution (to P_S) of first term in the summation of Eq. (68) yielding T (at $k = 2m$) is equal to zero. The same can be shown as below.

We consider $k = 2m$ in Eq. (68) and obtain Eq. (79) as below

$$T_{2m} = \overline{\gamma}\sqrt{b}S_{2m}\left(-\frac{1}{b\overline{\gamma}}\right)^{2m}\Gamma\left(2m-\frac{1}{2}\right) \tag{79}$$

where, S_{2m} can further be deduced from Eq. (69) and expressed as shown in Eq. (80).

$$\begin{aligned}S_{2m} &= \frac{1}{2m!}\left(\left(\frac{1}{\omega_2\sigma_p}+\frac{1}{\omega_1\sigma_t}\right)^{2m} - \sum_{l=0}^{m-1}\binom{2m}{l}\left(\frac{1}{\omega_2\sigma_p}\right)^l\right. \\ &\cdot\left(\frac{1}{\omega_1\sigma_t}\right)^{2m-l} \\ &\left.-\sum_{l=m+1}^{2m}\binom{2m}{l}\left(\frac{1}{\omega_2\sigma_p}\right)^l\left(\frac{1}{\omega_1\sigma_t}\right)^{2m-l}\right) \\ &= \frac{1}{2m!}\left(\left(\frac{1}{\omega_2\sigma_p}+\frac{1}{\omega_1\sigma_t}\right)^{2m} - \left(\frac{1}{\omega_2\sigma_p}+\frac{1}{\omega_1\sigma_t}\right)^{2m}\right) \\ &= 0\end{aligned} \tag{80}$$

Thus, using Eq. (80) in Eq. (79), we obtain Eq. (81) which showcases zero contribution of T (at $k = 2m$) to P_S in Eq. (67).

$$T_{2m} = 0 \tag{81}$$

By starting the summation in Eq. (68) from $k = 2m+1$ instead of $k = 2m$, we therefore obtain Eq. (82).

$$T = \overline{\gamma}\sqrt{b}\sum_{k=2m+1}^{\infty}S_k\left(-\frac{1}{b\overline{\gamma}}\right)^k\Gamma\left(k-\frac{1}{2}\right) \tag{82}$$

Moreover, with $\overline{\gamma}\to\infty$, the contribution to T (consisting of an infinite series) is primarily due to lower order terms. It is sufficient to only consider T at $k = 2m+1$ in the asymptotic (high SNR) regime [12]. By applying this in Eq. (82), we deduce Eq. (83) as below.

$$T^{\infty} = \overline{\gamma}\sqrt{b}S_{2m+1}\left(-\frac{1}{b\overline{\gamma}}\right)^{2m+1}\Gamma\left(2m+\frac{1}{2}\right) \tag{83}$$

Further, we utilize Eq. (66) to calculate S_{2m+1} by setting $k = 2m+1$ and obtain Eq. (84).

$$S_{2m+1} = \sum_{l=m}^{m+1}\frac{\left(\frac{1}{\omega_2\sigma_p}\right)^l\left(\frac{1}{\omega_1\sigma_t}\right)^{2m+1-l}}{l!(2m+1-l)!} \tag{84}$$

On solving Eq. (84), we further express S_{2m+1} as shown in Eqs. (85) and (86).

$$\Rightarrow S_{2m+1} = \frac{\left(\frac{1}{\omega_2\sigma_p}\right)^m\left(\frac{1}{\omega_1\sigma_t}\right)^{m+1}}{m!(m+1)!} + \frac{\left(\frac{1}{\omega_2\sigma_p}\right)^{m+1}\left(\frac{1}{\omega_1\sigma_t}\right)^m}{(m+1)!m!} \tag{85}$$

$$\Rightarrow S_{2m+1} = \frac{\left(\frac{1}{\omega_2\sigma_p}\right)^m\left(\frac{1}{\omega_1\sigma_t}\right)^{m+1} + \left(\frac{1}{\omega_2\sigma_p}\right)^{m+1}\left(\frac{1}{\omega_1\sigma_t}\right)^m}{m!(m+1)!} \tag{86}$$

Using Eq. (86) in Eq. (83), we obtain Eq. (87) as below.

$$T^{\infty} = \overline{\gamma}\sqrt{b}\frac{\left(\frac{1}{\omega_2\sigma_p}\right)^m\left(\frac{1}{\omega_1\sigma_t}\right)^{m+1} + \left(\frac{1}{\omega_2\sigma_p}\right)^{m+1}\left(\frac{1}{\omega_1\sigma_t}\right)^m}{m!(m+1)!} \cdot \left(-\frac{1}{b\overline{\gamma}}\right)^{2m+1}\Gamma\left(2m+\frac{1}{2}\right) \tag{87}$$

Further, Eq. (87) can be re-written as Eq. (88).

$$T^{\infty} = \overline{\gamma}\sqrt{b}\left(-\frac{1}{b\overline{\gamma}}\right)^{2m}\left(-\frac{1}{b\overline{\gamma}}\right)\Gamma\left(2m+\frac{1}{2}\right) \cdot \frac{\left(\frac{1}{\omega_2\sigma_p}\right)^m\left(\frac{1}{\omega_1\sigma_t}\right)^{m+1} + \left(\frac{1}{\omega_2\sigma_p}\right)^{m+1}\left(\frac{1}{\omega_1\sigma_t}\right)^m}{m!(m+1)!} \tag{88}$$

Subsequently, we obtain Eqs. (89) and (90) from Eq. (88) upon mathematical simplification.

$$T^{\infty} = -\frac{(\overline{\gamma b})^{-2m}\Gamma(2m+\frac{1}{2})}{\sqrt{b}m!(m+1)!}\left(\left(\frac{1}{\omega_2\sigma p}\right)^m\left(\frac{1}{\omega_1\sigma t}\right)^{m+1} + \left(\frac{1}{\omega_2\sigma p}\right)^{m+1}\left(\frac{1}{\omega_1\sigma t}\right)^m\right) \tag{89}$$

$$\Rightarrow T^{\infty} = \frac{(\overline{\gamma b})^{-2m}\Gamma(2m+\frac{1}{2})}{\sqrt{b}m!(m+1)!}\frac{1}{det(\Omega)^m(\sigma_p\sigma_t)^m} \cdot \left(\frac{1}{\omega_1\sigma_t}+\frac{1}{\omega_2\sigma_p}\right) \tag{90}$$

Replacing Eq. (90) into Eq. (67), we obtain the asymptotic (high SNR) SER shown in Eq. (91).

$$P_S^{\infty} = \frac{a\Gamma(2m+\frac{1}{2})(\overline{\gamma}b)^{-2m}\tilde{S}}{2\sqrt{\pi}m!(m+1)!\Delta_2(\Omega)\Delta_m(\Sigma)det(\Omega)^{m-1}} \tag{91}$$

Here, $\tilde{S}$ is represented using Eq. (92).

$$\tilde{S} = \sum_{p=1}^{m}\sum_{t=1,t\neq p}^{m}(-1)^{p+\phi(t)}\frac{\Delta_{m-2}\left(\sigma^{[p,t]}\right)}{\sigma_p\sigma_t} \times\left(\frac{1}{\omega_1\sigma_t}+\frac{1}{\omega_2\sigma_p}\right) \tag{92}$$

Further, it is noteworthy to state Eqs. (93) and (94).

$$\sum_{p=1}^{m}\sum_{t=1,t\neq p}^{m}(-1)^{p+\phi(t)}\frac{\Delta_{m-2}\left(\sigma^{[p,t]}\right)}{\sigma_p\sigma_t^2} = Le\left[(-1)^{m-2}\Delta_m(\sum)\right] \tag{93}$$

$$\sum_{p=1}^{m}\sum_{t=1,t\neq p}^{m}(-1)^{p+\phi(t)}\frac{\Delta_{m-2}\left(\sigma^{[p,t]}\right)}{\sigma_p^2\sigma_t} = Le\left[(-1)^{m-1}\Delta_m(\sum)\right] \tag{94}$$

where, $Le[\cdot]$ denotes well-known Laplace Expansion [11]. The derivations leading to Eqs. (93) and (94) are straightforward and have been omitted thereby. Using Eqs. (93) and (94) in Eq. (92), we deduce for $\tilde{S}$ as follows.

$$\tilde{S} = -\left(\frac{1}{\omega_1}\frac{1}{\omega_2}\right)\frac{\Delta_m(\sum)}{det(\sum)^2}$$
$$\Rightarrow \tilde{S} = -\frac{\Delta_2(\Omega)\Delta_m(\Sigma)}{det(\Omega)det(\sum)^2} \tag{95}$$

where, the well-established identity presented in Eq. (52) of our baseline work [10] is utilized to obtain the finalized $\tilde{S}$ expression shown in Eq. (95) [12], [15]. Finally, applying Eq. (95) into Eq. (91), we obtain the desired asymptotic (high SNR) SER closed form expression for MM wave MIMO-MRC model under double correlated Rayleigh (NLOS) channels in Eq. (96) [5], [10], [11].

$$\left(P_{S,MM}\right)_{hi}^{\infty} = \frac{a(4m-1)!!\cdot\overline{\gamma}^{-2m}}{b^{2m}2^{2m+1}m!(m+1)!det(\Omega)^m det(\sum)^2} \tag{96}$$

ACKNOWLEDGMENT

The authors would like to thank the Indian Institute of Information Technology Guwahati (IIITG) for facilitating the research.

REFERENCES

[1] S. Hur, T. Kim, D. J. Love, J. V. Krogmeier, T. A. Thomas, and A. Ghosh, "Millimeter wave beamforming for wireless backhaul and access in small cell networks," *IEEE Trans. Commun.*, vol. 61, no. 10, pp. 4391–4403, Oct. 2013.

[2] G. J. M. Janssen, B. C. van. Lieshout, and R. Prasad, "BER performance of millimeter wave indoor communication systems using multiple antenna signals," in *Proc. IEEE GLOBECOM. Commun., Global Bridge*, Oct. 1994, pp. 1075–1102.

[3] M. R. Andrews, P. P. Mitra, and R. deCarvalho, "Tripling the capacity of wireless communications using electromagnetic polarization," *Nature*, vol. 409, no. 6818, pp. 316–318, Jan. 2001.

[4] IEEE Spectrum. (Nov. 7, 2016). *Millimeter Waves Travel More Than 10 Kilometers in Rural Virginia 5G Experiment*. Accessed: Jan. 11, 2020. [Online]. Available: https://spectrum.ieee.org/tech-talk/telecom/wireless/millimeter-waves-travel-more-than-10-kilometers-in-rural-virginia

[5] R. W. Heath, N. González-Prelcic, S. Rangan, W. Roh, and A. M. Sayeed, "An overview of signal processing techniques for millimeter wave MIMO systems," *IEEE J. Sel. Topics Signal Process.*, vol. 10, no. 3, pp. 436–453, Apr. 2016.

[6] Y. Niu and Y. Li, "A survey of millimeter wave (mmWave) communications for 5G: Opportunities and challenges," *IEEE Trans. Wireless Commun.*, vol. 50, no. 4, pp. 532–535, Sep. 2002.

[7] Y. Song, S. D. Blostein, and J. Cheng, "Exact outage probability for equal gain combining with cochannel interference in Rayleigh fading," *IEEE Trans. Wireless Commun.*, vol. 2, no. 5, pp. 865–870, Sep. 2003.

[8] P. Hannan, "The element gain paradox for a phased-array antenna," *IEEE Trans. Antennas Propag.*, vol. 12, no. 4, pp. 423–433, 1964.

[9] T. S. Rappaport, "Broadband millimeter-wave propagation measurements and models using adaptive-beam antennas for outdoor urban cellular communication," *IEEE Trans. Antennas Propag.*, vol. 61, no. 4, pp. 1850–1860, Sep. 2013.

[10] M. R. McKay, A. J. Grant, and I. B. Collings, "Performance analysis of MIMO-MRC in double-correlated Rayleigh environments," *IEEE Trans. Commun.*, vol. 55, no. 3, pp. 497–507, Mar. 2007.

[11] R. S. Kshetrimayum, *Fundamentals of MIMO Wireless Communications*. Cambridge, U.K.: Cambridge Univ. Press, 2017.

[12] M. R. Akdeniz, Y. Liu, M. K. Samimi, S. Sun, S. Rangan, T. S. Rappaport, and E. Erkip, "Millimeter wave channel modeling and cellular capacity evaluation," *IEEE J. Sel. Areas Commun.*, vol. 32, no. 6, pp. 1164–1179, Jun. 2014.

[13] Rohde and Schwarz. (Oct. 25, 2014). *5G Technology*. Accessed: Sep. 23, 2015. [Online]. Available: www.rohdeschwarz.com/en/solutions/wireless-communications/5g/5g-fundamentals/5g-fundamentals_229439.html

[14] Engineering and Technology History Wiki. (Apr. 12, 2017). *Millimeter Waves*. Accessed: Jan. 5, 2020. [Online]. Available: https://ethw.org/Millimeter_Waves

[15] A. K. Jagannatham, "MATLAB project course on design and performance analysis of 5G wireless systems: mmWave, massive MIMO, NOMA, FBMC, full duplex and IoT," Dept. Elect. Eng., IIT Kanpur, India, Nov. 2019. [Online]. Available: https://home.iitk.ac.in/ adityaj/Teaching.html

[16] S. Srivastava, A. Mishra, A. Rajoriya, A. K. Jagannatham, and G. Ascheid, "Quasi-static and time-selective channel estimation for block-sparse millimeter wave hybrid MIMO systems: Sparse Bayesian learning (SBL) based approaches," *IEEE Trans. Signal Process.*, vol. 67, no. 5, pp. 1251–1266, Mar. 2019.

[17] A. Chawla, A. Patel, A. K. Jagannatham, and P. K. Varshney, "Distributed detection in massive MIMO wireless sensor networks under perfect and imperfect CSI," *IEEE Trans. Signal Process.*, vol. 67, no. 15, pp. 4055–4068, Aug. 2019.

[18] A. Kudeshia, A. K. Jagannatham, and L. Hanzo, "Total variation based joint detection and state estimation for wireless communication in smart grids," *IEEE Access*, vol. 7, pp. 31598–31614, 2019.

[19] P. Singh, H. B. Mishra, A. K. Jagannatham, K. Vasudevan, and L. Hanzo, "Uplink sum-rate and power scaling laws for multi-user massive MIMO-FBMC systems," *IEEE Trans. Commun.*, vol. 68, no. 1, pp. 161–176, Jan. 2020.

[20] P. Singh, H. B. Mishra, A. K. Jagannatham, and K. Vasudevan, "Semi-blind, training, and data-aided channel estimation schemes for MIMO-FBMC-OQAM systems," *IEEE Trans. Signal Process.*, vol. 67, no. 18, pp. 4668–4682, Sep. 2019.

[21] A. Agrahari, P. Varshney, and A. K. Jagannatham, "Precoding and downlink beamforming in multiuser MIMO-OFDM cognitive radio systems with spatial interference constraints," *IEEE Trans. Veh. Technol.*, vol. 67, no. 3, pp. 2289–2300, Mar. 2018.

[22] N. K. D. Venkategowda, B. B. Narayana, and A. K. Jagannatham, "Precoding for robust decentralized estimation in coherent-MAC-based wireless sensor networks," *IEEE Signal Process. Lett.*, vol. 24, no. 2, pp. 240–244, Feb. 2017.

[23] T. S. Rappaport, R. C. Daniels, R. W. Heath, Jr., and J. N. Murdock, "Introduction to millimeter wave wireless communications," informIT, Oct. 2014, pp. 1–32.

[24] Qualcomm. (Nov. 8, 2019). *QTM052 mmWave Antenna Modules*. Accessed: Jan. 10, 2020. [Online]. Available: https://www.qualcomm.com/products/qtm052-mmwave-antenna-modules

[25] J. Sharony, "Introduction to wireless MIMO: Theory and applications," in *Centre of Excellence in Wireless and IT: IEEE LI*. Stony Brook, NY, USA: Stony Brook Univ., Nov. 2006.

[26] H. Huang, C. B. Papadias, and S. Venkatesan, *MIMO Communications for Cellular Networks*. Cham, Switzerland: Springer, 2012.

[27] E. Biglieri, *MIMO Wireless Communications*. Cambridge, U.K.: Cambridge Univ. Press, 2007.

[28] H. Wymeeresch, *Iterative Receiver Design*. Cambridge, U.K.: Cambridge Univ. Press, 2007.

[29] A. Papoulis and S. U. Pillai, *Probability, Random Variables and Stochastic Processes*. New York, NY, USA: McGraw-Hill, 2002.

[30] A. Paulraj, R. Nabar, and D. Gore, *Introduction to Space-Time Wireless Communications*. Cambridge, U.K.: Cambridge Univ. Press, 2003.

[31] N. Costa and S. Haykin, *Mulitple-Input Multiple-Output Channel Models*. Hoboken, NJ, USA: Wiley, 2010.

[32] J. P. Kermoal, L. Schumacher, K. I. Pedersen, P. E. Mogensen, and F. Frederiksen, "A stochastic MIMO radio channel model with experimental validation," *IEEE J. Sel. Areas Commun.*, vol. 20, no. 6, pp. 1211–1226, Aug. 2002.

[33] J. G. Andrews, T. Bai, M. N. Kulkarni, A. Alkhateeb, A. K. Gupta, and R. W. Heath, "Modeling and analyzing millimeter wave cellular systems," *IEEE Trans. Commun.*, vol. 65, no. 1, pp. 403–430, Jan. 2017.

[34] W. Liu, "Adaptive wideband beamforming with sensor delay-lines," *Int. J. Signal Process.*, vol. 89, no. 5, pp. 876–882, May 2009.

[35] J. Litva and T. K. Lo, *Digital Beamforming in Wireless Communications*, 1st ed. Norwood, MA, USA: Artech House, 1996.

[36] X. Su and K. Chang, "Polarized uniform linear array system: Beam radiation pattern, beamforming diversity order, and channel capacity," *Int. J. Antennas Propag.*, vol. 2015, pp. 1–9, Oct. 2015.

[37] J. Okkonen, "Uniform linear adaptive antenna array beamforming implementation with a wireless open-access research platform," M.S. thesis, Dept. Comput. Sci. Eng., Univ. Oulu, Oulu, Finland, 2013, p. 58.

[38] W. Jeon and S.-Y. Chung, "The capacity of wireless channels: A physical approach," in *Proc. IEEE Int. Symp. Inf. Theory*, Jul. 2013, pp. 3045–3049.

[39] B. Friedlander and S. Scherzer, "Beamforming versus transmit diversity in the downlink of a cellular communications system," *IEEE Trans. Veh. Technol.*, vol. 53, no. 4, pp. 1023–1034, Jul. 2004.

[40] G. J. Foschini and M. J. Gans, "On limits of wireless communications in a fading environment when using multiple antennas," *Wireless Pers. Commun.*, vol. 6, no. 3, pp. 311–335, 1998.

[41] P. Nagaradjane and T. Muthu, "Performance of uplink feedback MIMO system using joint transmitter-receiver and polarization-multiplexing," *Comput. Electr. Eng.*, vol. 53, pp. 394–408, Jul. 2016.

[42] G. Aruna and S. Bhattacharyya, "Capacity and SNR analysis of a millimeter wave cellular network with phased antenna array," in *Proc. Int. Conf. Comput. Commun. Informat. (ICCCI)*, Jan. 2018, pp. 1–5.

[43] M. A. Halim, *Adaptive Array Measurements in Communications*, 1st ed. Norwood, MA, USA: Artech House, 2001.

[44] G. Tsoulos, M. Beach, and J. McGeehan, "Wireless personal communications for the 21st century: European technological advances in adaptive antennas," *IEEE Commun. Mag.*, vol. 35, no. 9, pp. 102–109, Oct. 1997.

[45] S. Drabowitch, H. G. Papiernik, and J. Encinas, *Modern Antennas*, 1st ed. London, U.K.: Chapman & Hall, 2005.

[46] W. Liu and S. Weiss, *Wideband Beamforming: Concepts and Techniques*. Hoboken, NJ, USA: Wiley, 2012.

[47] K. Jeon, X. Su, B. Hui, and K. Chang, "Practical and simple wireless channel models for use in multipolarized antenna systems," *Int. J. Antennas Propag.*, vol. 2014, pp. 1–10, Feb. 2014.

[48] R. S. Elliot, "Beamwidth and directivity of large scanning arrays," *Microw. J.*, pp. 74–82, 1964.

[49] A. E. Zooghby, *Smart Antenna Engineering*, 1st ed. Norwood, MA, USA: Artech House, 2005.

[50] K. S. Ahn, "Performance analysis of MIMO-MRC system in the presence of multiple interferers and noise over Rayleigh fading channels," *IEEE Trans. Wireless Commun.*, vol. 8, no. 7, pp. 3727–3735, Jul. 2009.

[51] D. Tse and P. Viswanath, *Fundamentals of Wireless Communication*. Cambridge, U.K.: Cambridge Univ. Press, 2005.

[52] A. S. Y. Poon and D. N. C. Tse, "Degree-of-freedom gain from using polarimetric antenna elements," *IEEE Trans. Inf. Theory*, vol. 57, no. 9, pp. 5695–5709, Sep. 2011.

[53] X. Su, B. Hui, and K. Chang, "3-D MIMO channel modeling with beamforming analysis for dual-polarized antenna systems," in *Proc. IEEE 78th Veh. Technol. Conf. (VTC Fall)*, Sep. 2013, pp. 1–5.

[54] W. Tan, S. D. Assimonis, M. Matthaiou, Y. Han, X. Li, and S. Jin, "Analysis of different planar antenna arrays for mmWave massive MIMO systems," in *Proc. IEEE 85th Veh. Technol. Conf. (VTC Spring)*, Jun. 2017, pp. 1–5.

[55] S. Zhu, H. Liu, and P. Wen, "A new method for achieving miniaturization and gain enhancement of Vivaldi antenna array based on anisotropic metasurface," *IEEE Trans. Antennas Propag.*, vol. 67, no. 3, pp. 1952–1956, Mar. 2019.

[56] E. G. Marin, "Planar array topologies for 5G communications in the Ku band," *IEEE Antennas Propag. Mag.*, vol. 61, no. 2, pp. 112–133, Aug. 2019.

[57] I.-J. Hwang, B. Ahn, S.-C. Chae, J.-W. Yu, and W.-W. Lee, "Quasi-Yagi antenna array with modified folded dipole driver for mmWave 5G cellular devices," *IEEE Antennas Wireless Propag. Lett.*, vol. 18, no. 5, pp. 971–975, May 2019, doi: 10.1109/LAWP.2019.2906775.

[58] M. M. S. Taheri, A. Abdipour, S. Zhang, and G. F. Pedersen, "Integrated millimeter-wave wideband end-fire 5G beam steerable array and low-frequency 4G LTE antenna in mobile terminals," *IEEE Trans. Veh. Technol.*, vol. 68, no. 4, pp. 4042–4046, Apr. 2019.

[59] E. H. Mujammami and A. B. Sebak, "Wideband high gain printed quasi-Yagi diffraction gratings-based antenna for 5G applications," *IEEE Access*, vol. 7, pp. 18089–18100, 2019.

[60] M. Khatun, H. Mehrpouyan, D. Matolak, and I. Guvenc, "Millimeter wave systems for airports and short-range aviation communications: A survey of the current channel models at mmWave frequencies," in *Proc. IEEE/AIAA 36th Digit. Avionics Syst. Conf. (DASC)*, Sep. 2017, pp. 1–8.

[61] M. K. Samimi, S. Sun, and T. S. Rappaport, "MIMO channel modeling and capacity analysis for 5G millimeter-wave wireless systems," in *Proc. 10th Eur. Conf. Antennas Propag. (EuCAP)*, Apr. 2016, pp. 1–5.

[62] I. A. Hemadeh, K. Satyanarayana, M. El-Hajjar, and L. Hanzo, "Millimeter-wave communications: Physical channel models, design considerations, antenna constructions, and link-budget," *IEEE Commun. Surveys Tuts.*, vol. 20, no. 2, pp. 870–913, 2nd Quart., 2018.
[63] T. S. Rappaport, Y. Xing, G. R. MacCartney, A. F. Molisch, E. Mellios, and J. Zhang, "Overview of millimeter wave communications for fifth-generation (5G) wireless networks—With a focus on propagation models," *IEEE Trans. Antennas Propag.*, vol. 65, no. 12, pp. 6213–6230, Dec. 2017.
[64] E. Turgut and M. C. Gursoy, "Average error probability analysis in mmWave cellular networks," in *Proc. IEEE 82nd Veh. Technol. Conf. (VTC-Fall)*, Sep. 2015, pp. 1–5.
[65] H. Zhang, "Diversity and equalization for MultiGigabit millimeter wave communications over a sparse multipath channel," Doctoral dissertation, Dept. Elect. Comput. Eng., Univ. California, Santa Barbara, CA, USA, Dec. 2012.
[66] K. Belbase, C. Tellambura, and H. Jiang, "Coverage, capacity, and error rate analysis of multi-hop millimeter-wave decode and forward relaying," *IEEE Access*, vol. 7, pp. 69638–69656, 2019.
[67] H. Bolcskei, M. Borgmann, and A. J. Paulraj, "Impact of the propagation environment on the performance of space-frequency coded MIMO-OFDM," *IEEE J. Sel. Areas Commun.*, vol. 21, no. 3, pp. 427–439, Apr. 2003.
[68] A. F. Molisch et al., "IEEE 802.15.4a channel model—Final report," in *Proc. IEEE 802.15.4a Channel Modeling Subgroup*, 2004.
[69] E. Bjornson, L. Van der Perre, S. Buzzi, and E. G. Larsson, "Massive MIMO in Sub-6 GHz and mmWave: Physical, practical, and use-case differences," *IEEE Wireless Commun.*, vol. 26, no. 2, pp. 100–108, Apr. 2019.
[70] H. Ganesan and S. C. Ghosh, "Evidential obstacle learning in millimeter wave D2D communication using spatial correlation," in *Proc. 14th Int. Conf. Commun. Syst. Netw. (COMSNETS)*, Bengaluru, India, Jan. 2022, pp. 344–352.
[71] C. B. Barneto, E. Rastorgueva-Foi, M. F. Keskin, T. Riihonen, M. Turunen, J. Talvitie, H. Wymeersch, and M. Valkama, "Millimeter-wave mobile sensing and environment mapping: Models, algorithms and validation," *IEEE Trans. Veh. Technol.*, vol. 71, no. 4, pp. 3900–3916, Apr. 2022.
[72] Y. Karasawa, "A multistate channel model composed of line-of-sight and semi-line-of-sight propagation environments for millimeter-wave mobile radio systems," *IEEE Trans. Antennas Propag.*, vol. 69, no. 12, pp. 8731–8743, Dec. 2021.
[73] W. Xia, S. Rangan, M. Mezzavilla, A. Lozano, G. Geraci, V. Semkin, and G. Loianno, "Millimeter wave channel modeling via generative neural networks," in *Proc. IEEE Globecom Workshops (GC Wkshps*, Dec. 2020, pp. 1–6.
[74] S. Ju, Y. Xing, O. Kanhere, and T. S. Rappaport, "Millimeter wave and sub-terahertz spatial statistical channel model for an indoor office building," *IEEE J. Sel. Areas Commun.*, vol. 39, no. 6, pp. 1561–1575, Jun. 2021.
[75] X. Zhao, Z. Fu, W. Fan, Y. Zhang, S. Geng, F. Du, P. Qin, Z. Zhou, and L. Zhang, "Semi-deterministic dynamic millimeter-wave channel modeling based on an optimal neural network approach," *IEEE Trans. Antennas Propag.*, vol. 70, no. 6, pp. 4082–4095, Jun. 2022.
[76] M. Lecci, M. Polese, C. Lai, J. Wang, C. Gentile, N. Golmie, and M. Zorzi, "Quasi-deterministic channel model for mmWaves: Mathematical formalization and validation," in *Proc. GLOBECOM IEEE Global Commun. Conf.*, Dec. 2020, pp. 1–6.
[77] N. Arafat and A. El-Mahdy, "Performance of fully digital zero-forcing precoding in mmWave massive MIMO-NOMA with antenna reduction," in *Proc. 30th Wireless Opt. Commun. Conf. (WOCC)*, Oct. 2021, pp. 166–170.
[78] W. Ahmad, H. Zhang, Y. Chen, and N. Iqbal, "Full digital transmit beamforming with low RF complexity for large-scale mmWave MIMO system," in *Proc. IEEE Int. Conf. Commun. (ICC)*, Dublin, Ireland, Jun. 2020, pp. 1–6.

SABYASACHI BHATTACHARYYA received the B.Tech. degree in electronics and communication engineering from the School of Technology, Assam Don Bosco University, Guwahati, Assam, the M.Tech. degree in signal processing and communication from Gauhati University, Guwahati, India, and the Ph.D. degree from the Indian Institute of Information Technology Guwahati (IIITG). His research interests include digital phased locked loops, DPLL based wireless communications, 5G MM wave communication systems, and channel models.

G. ARUNA received the Ph.D. degree from the Indian Institute of Technology Guwahati (IITG). She is currently working as an Assistant Professor with the Department of Electronics and Communication Engineering, Indian Institute of Information Technology Guwahati (IIITG). Her research interests include wireless and mobile communications, MIMO systems, and MM wave communications.